ABSTRACT

Title of Thesis: REAL-TIME COMPARISON OF PHYSICAL AND CHEMICAL AEROSOL MEASUREMENT METHODS

Francis Oyebanjo, Master of Science, 2019

Thesis directed by: Dr. Akua Asa-Awuku
Department of Chemical Engineering

Atmospheric aerosols are major contributors to air pollution. Overexposure to these particles can cause severe respiratory and cardiovascular impairments. Aerosols also affect the planet's climate through radiative forcing. Various techniques exist to monitor the physical and chemical characteristic of aerosols but few allow for real-time analysis. In this thesis, real-time field measurements of aerosol particles were compared with values reported by state regulatory agencies. These values were also compared to mass concentrations of $PM_{2.5}$ in order to determine if a correlation exists between the two. Lastly, the relationship between particle mobility-size and chemical characterization using Raman spectroscopy is explored in an effort to obtain quantitative semi-continuous spectral data. This study found no variation between local and regional particulate matter measurements and no discernable correlation between $PM_{2.5}$ mass and particle number concentration. The relationship between particle size and Raman intensity remains unknown due to the non-uniformity of mobility-size selected particles.

REAL-TIME COMPARISON OF PHYSICAL AND CHEMICAL AEROSOL MEASURMENT METHODS

by

Francis Oyebanjo

Thesis submitted to the Faculty of the Graduate School of the
University of Maryland, College Park, in partial fulfillment
of the requirements for the degree of
Master of Science
2019

Advisory Committee:
Professor Akua Asa-Awuku, Chair/Advisor
Professor Ganesh Sriram
Professor Dongxia Liu

Dedication

To my parents, Olakunle and Roseline Oyebanjo, my siblings, Michael and Anthony Oyebanjo and Samuel and Oluwadamilola Osobu. To my nephew, Joshua Osobu, and to all the members of the Young Black Professional founding class.

Acknowledgements

I would like to thank my advisor, Dr. Akua Asa-Awuku for her constant guidance, continued encouragement, and overwhelming support throughout the duration of my graduate studies. I would also like to than Dr. Emmanuel Fofie for his initial training on the use and inner workings of all the laboratory instruments. I would like to thank Dr. Qi Yao for always being there to help answer my questions. I would also like to thank all the other members of the Environmental Aerosol Research Lab Group. I have enjoyed my time with all of you and have learned a great deal.

I'd like to thank my other mentors, Dr. David Doughty and Dr. Steven Hill of the Army Research lab for allowing me to work with them extensively over the course of the last year. I have gained an immeasurable amount of knowledge and am grateful for everything I have learned from the two of you. I would also like to thank everyone at the Army Research lab who made my time there over the summer enjoyable.

I would like to thank Phillip Stratton from the UMD Atmospheric and Oceanic Sciences Department for all his help in conducting my experiments and Dr. Russel Dickerson for allowing us to use his rooftop laboratory space. I would also like to thank Ryan Auvill, Colleen Williams, Adam Reese, Willis Fotiadis and Aaron Ryan, at the Maryland Department of the Environment for allowing me to access and utilize their facilities while conducting my research.

I would like to express my immeasurable gratitude to the UMD Louis Stokes Alliance for Minority Participation (LSAMP) Bridge to the Doctorate Fellowship and the National Science Foundation for funding my graduate studies. I would also like to thank the former LSAMP directors Ms. Michelle Udeli and Dr. Sarah Mburu for helping facilitate my interest in research during the LSAMP Undergraduate Research Program. I would also like to thank Ms. Rosemary Parker, Director of the Center for Minorities in Sciences and Engineering, for her continued guidance and support.

I would like to thank my loving family and friends for their consistent love, support, and genuine desire for me to succeed. Last but not least, I would like to thank God for his never ending blessings over my life.

Table of Contents

Dedication ii

Acknowledgements iii

Table of Contents v

List of Tables vii

List of Figures viii

List of Abbreviations x

Chapter 1: Introduction 1

1.1 What are aerosols? 1
1.2 Impact of Aerosols 2
1.3 Measurement Methods 10
1.4 Overview of thesis 14
1.4.1 Objective 14
1.4.2 Particle Sizing 15
1.4.3 Lab Measurements 17

Chapter 2: Field Measurements & Physical Aerosol Detection Measurements 20

2.1 Research Objectives 20
2.2 Methodology 23
2.3 Results 27
2.4 Discussion 32
2.5 Conclusion 39

Chapter 3: Chemical Characterization of Aerosol Particles Using Raman Spectroscopy 41

3.1 Overview 41
3.1.1 Black Carbon 41
3.1.2 Chemical Measurement Methods 42
3.1.3 Raman Spectroscopy 44
3.2 Methodology 46
3.3 Results & Discussion 49
3.3.1 Control Particles 49
3.3.2 Dry BC Sampling 52
3.3.3 BC Atomization 58

Chapter 4: Conclusions and Future Work 62

4.1 Conclusions 62

4.2 Recommendations for Future Work 63
Appendix A: Additional Figures from Field Measurements 65

Appendix B: Additional Raman Spectra Images 70

Bibliography 72

Presentations 78

List of Tables

Table 1.2.1 National Ambient Air Quality Standards (NAAQs) (US EPA 2014) 6

Table 1.2.2 European Union Air Quality Standards ("Standards - Air Quality - Environment - European Commission" 2018) 7

Table 1.2.3 China's Air Quality Standards ("China: Air Quality Standards | Transport Policy" 2018) 9

Table 1.2.4 European Union Motor Vehicle Emissions Standards for cars and passenger Vehicles ("Emission Standards: Europe: Cars and Light Trucks" n.d.) 9

Table 1.2.5 European Union Motor Vehicle Emissions Standards for Light Commercial Vehicles ("Emission Standards: Europe: Cars and Light Trucks" n.d.) 10

Table 1.4.1 CPC Comparison... 18

List of Figures

Figure 1.3.1 Particle volume ($n°_V$), surface area ($n°_S$), and number ($n°_N$) concentrations of urban aerosol as a function of particle diameter (Seinfeld and Pandis 2016). 12

Figure 1.3.2 Basic Water CPC Schematic (TSI) 13

Figure 1.4.1 Average Particle Concentration from Room Air (left) and Atomized Ammonium Sulfate (right) 18

Figure 1.4.2 Butanol vs. Water CPC Black Carbon Particle Sizing Comparison 19

Figure 2.1.1 Map of Air Monitoring Stations in Maryland (Users et al. 2018) 20

Figure 2.1.2 Satellite View of PG Equestrian Center Air Monitoring Station (Users et al. 2018) 21

Figure 2.1.3 Satellite View of HU-Beltsville Air Monitoring Station (Users et al. 2018) 22

Figure 2.1.4 Distance between College Park and HU-Beltsville Sampling Locations 23

Figure 2.2.1 CPC Sampling Flow Schematic 24

Figure 2.2.2 HU-Beltsville CPC Sampling Flow Schematic with DMA attached 25

Figure 2.2.3 CPC College Park CPC Flow Schematic with DMA Attached 26

Figure 2.3.1 CPC Particle Count Comparison from HU-Beltsville Monitoring Station 28

Figure 2.3.2 CPC Particle Count Comparison from College Park Monitoring Station with Simultaneous with Simultaneous Measurements from HU-Beltsville 29

Figure 2.3.3 Particle Size Distribution Time Series from College Park Sampling 30

Figure 2.3.4 Particle Size Distribution Time Series from HU-Beltsville Sampling 31

Figure 2.3.5 CPC Particle Count Comparison from HU-Beltsville Monitoring Station during Particle Size Distribution Sampling 32

Figure 2.4.1 One-to-One CPC Particle Count Comparison of TSI 3776 and TSI 3772 at from HU-Beltsville Monitoring Station 33

Figure 2.4.2 One-to-One CPC Particle Count Comparison of TSI 3776 and Teledyne 651 at from HU-Beltsville Monitoring Station 34

Figure 2.4.3 One-to-One CPC Particle Count Comparison of TSI 3776 and Teledyne 651 at College Park and Beltsville Locations 35

Figure 2.4.4 CPC Particle Count Comparison from HU-Beltsville Monitoring Station with $PM_{2.5}$ mass concentrations reported by the MDE 37

Figure 2.4.5 Hourly $PM_{2.5}$ mass concentration at HU-Beltsville as a function TSI 3776 Ultrafine Butanol CPC Number Concentration 38

Figure 3.2.1 Flow Configuration of Dry BC Sampling 49

Figure 3.2.2 Flow Configuration of Wet BC Sampling 49
Figure 3.3.2 Single Raman spectra taken during sampling of 300nm PSL particles 51
Figure 3.3.3 Raman Spectra Comparison of 300nm PSL Nanospheres (images from 7 particles selected in figure 3.3.2) 52
Figure 3.3.4 Raman Intensity Image of 300nm Printex® Particles 53
Figure 3.3.5 Single Raman spectra taken during sampling of 300nm PSL particles 54
Figure 3.3.6 Raman Spectra Comparison of 300nm Printex® 55
Figure 3.3.7 SEM Photograph of 300nm Printex® 56
Figure 3.3.9 Raman Intensity Image and selected Raman Spectra of 300nm Size selected Wax Candle Burn Particles 57
Figure 3.3.10 Raman Intensity Image and selected Raman Spectra of 500nm Size selected Cellulose Burn 57
Figure 3.3.11 Raman Intensity Image of 300nm Atomized Printex® (random particles selected in white) 58
Figure 3.3.12 Selected Raman Spectra of 300nm Atomized Printex® Particles 59
Figure 3.3.13 SEM Photograph of 300nm Atomized Printex® Particles at scales of 10µm (A) and 1µm (B) 59
Figure A.1. Feb 25th -Feb 27th Particle Size Distribution at College Park Lab (12 Hour Avg.) Top, (Day/Night Avg.) Bottom 65
Figure A.2. Mar 26th -Feb 27th Particle Size Distribution at College Park Lab (12 Hour Avg.) Top, (Day/Night Avg.) Bottom 66
Figure A.3 Ozone and $PM_{2.5}$ Pollutant Concentration Reported During Sampling Periods 67
Figure A.4 Ratio of Number Concentration recorded between CPC's During Sampling Periods 68
Figure A.5. Difference in Number Concentration recorded between CPC's During Sampling Periods 69
Figure B.1. SEM Image of 300nm Mobility Size Selected PSL 70
Figure B.2. Raman Intensity Image of 100nm (Atomized) Printex® Particles 70
Figure B.3. Raman Intensity Image and Selected Raman Spectra of 300nm Ambient Air Particles 71

List of Abbreviations

AAC	Aerodynamic Aerosol Classifier
BC	Black Carbon
C_{brown}	Brown Carbon
CP	College Park, MD
CCD	Charge Coupled Device
CPC	Condensation Particle Counter
DMA	Differential Mobility Analyzer
EC	Elemental Carbon
EPA	Environmental Protection Agency
FTIR	Fourier Transform Infrared Spectroscopy
HU	Howard University
IR	Infrared Spectroscopy
MDE	Maryland Department of the Environment
NAAQS	National Ambient air Quality Standards
PM	Particulate Matter
PM_{10}	Particulate Matter less than 10 microns
$PM_{2.5}$	Particulate Matter less than 2.5 microns
PN	Particle Number Concentration
PSD	Particle size Distribution
PTFE	polytetrafluoroethylene
RS	Raman Spectroscopy
SMPS	Scanning Mobility Particle Sizer

Chapter 1: Introduction

1.1 What are aerosols?

Aerosols are typically characterized as the suspension of some liquid or solid particle in a gaseous medium (Kulkarni, Baron, and Willeke 2011). They can be formed through the physical or chemical breakdown of a liquid or solid into smaller parts. Many natural processes lead to the formation of aerosols. For example, material emitted during volcanic eruptions, sand and dust blown from desserts, and salt particles from ocean waves are just a few examples of aerosols formed through ecological events (Kulkarni, Baron, and Willeke 2011). Organisms can also produce aerosols through various biological processes. Terpenes are a class of organic compounds emitted by a variety of plant and animal species to protect them from predators and attract more beneficial organisms (Gershenzon and Dudareva 2007). Isoprenes, the most abundant atmospheric terpene, are organic compounds emitted by trees and phytoplankton located in marine environments. These terpenes are known to react with other chemicals in the atmosphere such as ozone and nitrous oxide to form aerosols (Moore, Oram, and Penkett 1994).

While various natural processes produce aerosols, many anthropogenic events are also responsible for aerosol emissions. The most recognizable form of aerosols are the pressure sealed cans used to disperse liquid or gaseous consumer products in the form of a mist, foam, or spray (National Aerosol Association 2014). Transportation emissions are perhaps the next most recognizable source of aerosols. Specifically, engine exhaust from diesel and gasoline fuel sources produce aerosols during the combustion process. These exhaust are responsible for the emission of both primary and secondary atmospheric particles (Jr et al. 1973). Primary aerosols are those that are present in the atmosphere in the original condensed phase (liquid or solid) at the time of emission; while secondary aerosols are formed through the physical or chemical breakdown of particles within the atmosphere. For example, gas-phase compounds can oxidize to form particles downwind of sources. Furthermore, the aerosols emitted in vehicle exhaust tend to be very fine particles (≤ 2.5 μm, $PM_{2.5}$) that have adverse implications on human health (Maricq, Podsiadlik, and Chase 2000). Additional anthropogenic aerosols sources include emissions from manufacturing and energy production using fossil fuels. Particles emitted during these processes are often co-emitted with pollutants such as carbon dioxide (CO_2), nitrous oxides (NO_x), sulfur oxides (SO_x), and various other compounds (Davis 2018).

1.2 Impact of Aerosols

Regardless of their source, aerosols eventually coagulate and disperse in the atmosphere and have major impacts on both human and environmental health. These particles have significant direct and indirect effects on the planets energy balance, cloud properties, and essential atmospheric chemical reactions (Tegen and Schepanski 2018). Directly, atmospheric aerosol particles absorb and reflect solar and thermal radiation (Lohmann and Feichter 2005 & references therein). The impact these absorption and reflection perturbations have on the planets energy balance are described as radiative forcing. The indirect effect is the phenomena observed when aerosol particles act as cloud condensation nuclei (CCN) for the formation of cloud droplets in the atmosphere (Lohmann and Feichter 2005 and references therein). Large concentrations of small aerosol particles provide more surface area for cloud droplets to condense upon. This leads to the formation of larger, brighter clouds that reflect sunlight and have a negative radiative forcing on the earth's atmosphere (U Lohmann and Feichter 2005; Charlson and Wigley 1994). Both the indirect and direct aerosol effect depend largely on the size, color, and composition of the particles.

For example, studies have shown that black and brown carbon aerosols produced in combustion processes such as biomass burning have a net atmospheric radiative forcing that is a function of the aerosol size distribution (Chylek and Wong 1995 & references therein). A study of Aerosol radiative forcing in the United States found that lighter particles such as SO_x and NO_x had a negative radiative forcing (cooling) while the darker, soot-like, black carbon particles had a net positive radiative forcing (heating) (Leibensperger et al. 2011 & references therein). However, it is important to remember that these light and dark particles are not separated in the atmosphere and likely interact with one another. These multi-aerosol compounds have unique effects on radiative forcing. For instance, sulfate can have a radiative forcing value as low as -2.0 W/m^2 (Leibensperger et al. 2011). However in one study, when sulfate and carbonaceous aerosol were externally mixed, the radiative forcing of the sulfate portion was nearly zero while the contribution of the carbonaceous material was -1.3 W/m^2 (Ulrike Lohmann et al. 2000).

It is necessary to point out that the environmental impact of aerosol emissions are not limited to the location of the emission source. Winds can carry aerosols thousands of miles away from their point of origin. Some organic aerosols can even react with precursor gases in the atmosphere and form secondary organic aerosols that lead to higher particulate concentration downwind of the emission source (Carlton, Wiedinmyer, and Kroll 2009).

While the scattering of aerosol particles due to wind may seem advantageous, meteorological and topographical features of certain regions may make this undesirable (Lu and Turco 1995). The Greater Los Angeles Metropolitan area is an example of one such region. Los Angeles is the second most populated city in the nation and as such, is subject to elevated levels of air pollutants including hydrocarbons (Haagen-Smit 1952). These hydrocarbons undergo photochemical reactions with other pollutants leading to the formation of a thick smog composed of aerosols, ozone, NO_x, and SO_x (David D. Parrish et al. 2016). One would expect the sea breeze from the nearby Pacific Ocean to disperse the smog. However, the city is located in a basin bounded by mountains to the east. Furthermore, topical inversion layers keep warmer air masses above the cooler, polluted ground air, which prevents the smog from vertically dispersing (Yang and Omaye 2009). The city has since taken steps to reduce pollution and other densely populated areas in the world ,such as Beijing, China, have studied Los Angeles closely in order to mitigate the effects of air pollution in their cities (David D. Parrish et al. 2016). This is largely due to the environmental and, more importantly, human cost that aerosol emissions can have. According to the World Health Organization, exposure to particulate matter (atmospheric aerosols) causes about 7 million deaths every year (Esposito et al. 2018)(Esposito et al. 2018. Size is of particular importance when discussing the emissions of particulate matter. Smaller particles are broken down into two categories, PM_{10} (particles less than 10 microns) and $PM_{2.5}$ (particles less than 2.5 microns). PM_{10} typically has short term effects on respiratory health while $PM_{2.5}$ can be much more dangerous. These very fine particles deposit in respiratory airways and lead to decreased lung function, difficulty breathing, and in the most severe cases, heart attacks (World Health Organization 2006).

In order to monitor the impact of these particles, regulatory agencies across the globe have set standards for acceptable levels of PM_{10} and $PM_{2.5}$. In the United States, the Environmental Protection Agency is the federal agency responsible for setting the acceptable levels of all criterion air pollutants. Individual state agencies are responsible for monitoring respective levels within their state and reporting when they are/are not in compliance. Similarly, the European Union's sets limits for the emissions of some criterion air pollutants and target emission rates for others

("Standards - Air Quality - Environment - European Commission" 2018). The worlds most populated countries, China and India have also issued air quality standards for its citizens to adhere to. In China, standards are issued for special regions such as national parks (Class 1) and other public and nonpublic areas (Class 2) ("China: Air Quality Standards | Transport Policy" 2018). Furthermore, population dense regions of the nation ,such as Beijing and Shanghai, were required to implement more stringent air quality standards in shorter timeframes ("China: Air Quality Standards | Transport Policy" 2018). In India, the Central Pollution Control Board, sets and regularly test air quality standards ("India: Air Quality Standards | Transport Policy" 2018). Tables 1.1-1.3 display the air quality standards for all air pollutants in the named regions. In all cases, particulate matter is listed as a criterion pollutant with distinction between PM_{10} and $PM_{2.5}$. Table's 1.4-1.5 display emission limits for heavy and light duty vehicles with particulate matter included.

Table 1.2.1 National Ambient Air Quality Standards (NAAQs) (US EPA 2014)

Pollutant		Primary/Secondary	Averaging Time	Level	Form
Carbon Monoxide (CO)		Primary	8 hours	9 ppm	Not to be exceeded more than once per year
			1 hour	35 ppm	
Lead (Pb)		Primary and Secondary	Rolling 3 month average	0.15 µg/m^3	Not to be exceeded
Nitrogen Dioxide (NO_2)		Primary	1 hour	100 ppb	98th percentile of 1-hour daily max concentrations, averaged over 3 years
		Primary and Secondary	1 year	53 ppb	Annual mean
Ozone (O_3)		Primary and Secondary	8 hours	0.070 ppm	Annual 4th highest daily max 8 hour concentration, averaged over 3 years
Particle Pollution (PM)	$PM_{2.5}$	Primary	1 year	12.0 µg/m3	annual mean, averaged over 3 years
		Secondary	1 year	15.0 µg/m3	annual mean, averaged over 3 years
		Primary and Secondary	24 hours	35 µg/m3	99th percentile averaged over 3 years
	PM_{10}	Primary and Secondary	24 hours	150 µg/m3	annual mean, averaged over 3 years
Sulfur Dioxide (SO_2)		Primary	1 hour	75 ppb	99th percentile of 1-hour daily max, averaged over 3 years
		Secondary	3 hour	0.5 ppm	Not to be exceeded more than once per year

Table 1.2.2 European Union Air Quality Standards ("Standards - Air Quality - Environment - European Commission" 2018)

Pollutant	***Concentration***	***Averaging period***	***Legal nature***	***Permitted exceedances each year***
Fine particles ($PM_{2.5}$)	25 µg/m3***	1 year	Target value to be met as of 1.1.2010 Limit value to be met as of 1.1.2015	n/a
Sulphur dioxide (SO2)	350 µg/m3	1 hour	Limit value to be met as of 1.1.2005	24
	125 µg/m3	24 hours	Limit value to be met as of 1.1.2005	3
Nitrogen dioxide (NO2)	200 µg/m3	1 hour	Limit value to be met as of 1.1.2010	18
	40 µg/m3	1 year	Limit value to be met as of 1.1.2010 *	n/a
PM_{10}	50 µg/m3	24 hours	Limit value to be met as of 1.1.2005 **	35
	40 µg/m3	1 year	Limit value to be met as of 1.1.2005 **	n/a
Lead (Pb)	0.5 µg/m3	1 year	Limit value to be met as of 1.1.2005 (or 1.1.2010 in the immediate vicinity of specific, notified industrial sources; and a 1.0 µg/m3 limit value applied from 1.1.2005 to 31.12.2009)	n/a
Carbon monoxide (CO)	10 mg/m3	Maximum daily 8 hour mean	Limit value to be met as of 1.1.2005	n/a
Benzene	5 µg/m3	1 year	Limit value to be met as of 1.1.2010**	n/a
Ozone	120 µg/m3	Maximum daily 8 hour mean	Target value to be met as of 1.1.2010	25 days averaged over 3 years
Arsenic (As)	6 ng/m3	1 year	Target value to be met as of 31.12.2012	n/a
Cadmium (Cd)	5 ng/m3	1 year	Target value to be met as of 31.12.2012	n/a
Nickel (Ni)	20 ng/m3	1 year	Target value to be met as of 31.12.2012	n/a

Pollutant	***Concentration***	***Averaging period***	***Legal nature***	***Permitted exceedances each year***
Polycyclic Aromatic Hydrocarbons	1 ng/m3 (expressed as concentration of Benzo(a)pyrene)	1 year	Target value to be met as of 31.12.2012	n/a

Table 1.2.3 China's Air Quality Standards ("China: Air Quality Standards | Transport Policy" 2018)

Pollutant	Averaging time	Limit		Unit
		Class 1	Class 2	
SO_2	annual	20	60	μg/m^3
	24 hours	50	150	
	hourly	150	500	
NO_2	annual	40	40	
	24 hours	80	80	
	hourly	200	200	
CO	24 hours	4	4	mg/m^3
	hourly	10	10	
O_3	daily, 8-hour maximum	100	160	μg/m^3
	hourly	160	200	
PM10	annual	40	70	
	24 hours	50	150	μg/m^3
$PM_{2.5}$	annual	15	35	
	24 hours	35	75	

Table 1.2.4 European Union Motor Vehicle Emissions Standards for cars and passenger Vehicles ("Emission Standards: Europe: Cars and Light Trucks" n.d.)

Stage	**Date**	**CO**	**HC**	**HC+NOx**	**NOx**	**PM**	**PN**
		g/km					**#/km**
Positive Ignition (Gasoline)							
Euro 6	2014.09	1.0	0.10[d]	-	0.06	0.005[e,f]	6.0×10^{11}
Compression Ignition (Diesel)							
Euro 5b	2011.09[c]	0.50	-	0.23	0.18	0.005[f]	6.0×10^{11}
Euro 6	2014.09	0.50	-	0.17	0.08	0.005[f]	6.0×10^{11}

Table 1.2.5 European Union Motor Vehicle Emissions Standards for Light Commercial Vehicles ("Emission Standards: Europe: Cars and Light Trucks" n.d.)

Category†	**Stage**	**Date**	**CO**	**HC+NOx**	**NOx**	**PM**	**PN**
			g/km				**#/km**
Compression Ignition (Diesel)							
N_1, Class I ≤1305 kg	Euro 5b	2011.09[d]	0.50	0.23	0.18	0.005[f]	6.0×10^{11}
	Euro 6	2014.09	0.50	0.17	0.08	0.005[f]	6.0×10^{11}
N_1, Class II 1305-1760 kg	Euro 5b	2011.09[d]	0.63	0.295	0.235	0.005[f]	6.0×10^{11}
	Euro 6	2015.09	0.63	0.195	0.105	0.005[f]	6.0×10^{11}
N_1, Class III >1760 kg	Euro 5b	2011.09[d]	0.74	0.350	0.280	0.005[f]	6.0×10^{11}
	Euro 6	2015.09	0.74	0.215	0.125	0.005[f]	6.0×10^{11}

1.3 Measurement Methods

All of the regulatory agencies listed rely on the mass concentration of particulate matter when measuring and reporting aerosol data. This is often done using some form of filter based, gravimetric sampling over extended periods of time (Tittarelli et al. 2008). Aerosol particles are sampled continuously onto the filter for a given time frame and then measured for physical or chemical properties once the filter is removed. However, the method of reporting particle concentration changes with the application of the data (Kulkarni, Baron, and Willeke 2011). Regulatory agencies, such as those above, typically rely on mass concentration (Kulkarni, Baron, and Willeke 2011). The EU is unique in its separate standards for vehicle particle emission limits reported in terms of particle number. Toxicological studies tend to require surface area concentration, particle counts are recorded in number concentration for clean rooms, and some engineering applications require volume concentration(Kulkarni, Baron, and Willeke 2011). These different concentrations can also be affected by the properties of the particles themselves. These properties include size, shape, cohesion, porosity, and charging. Figure 1.3.1 illustrates the variations seen when particle size and concentration are measured using different methods. In this figure the, volume ($n°_V$), surface area ($n°_S$), and number ($n°_N$) concentrations of the particles are depicted using logarithmic plots. The x-axis is the logarithm of the midpoint particle diameter in a given size bin. Particle sizes can vary significantly so they are often grouped into size bins rather than average sizes. The y-axis represents is the change in concentration over the change in the particle size in a given size bin, also known as d $n°_i$ /dlogDp. Particle size distributions are reported using these conventions because they often results in the Gaussian distribution of particle sizes. However the type of concentration reported dictates the particle sizes the distribution will include. Number concentrations are skewed toward smaller particles. Surface area is also skewed slightly towards smaller particles since the large number of fine particles would likely lead to increased surface area. However volume (mass) concentration is skewed towards the larger particle diameters and even exhibits a bimodal distribution. In the surface area and number measurements, the larger particle sizes represent only the insignificant tail end of the distribution. The particles that have the most impact on the environment and human health are the smaller particles that are represented on the lower end of the size distribution.

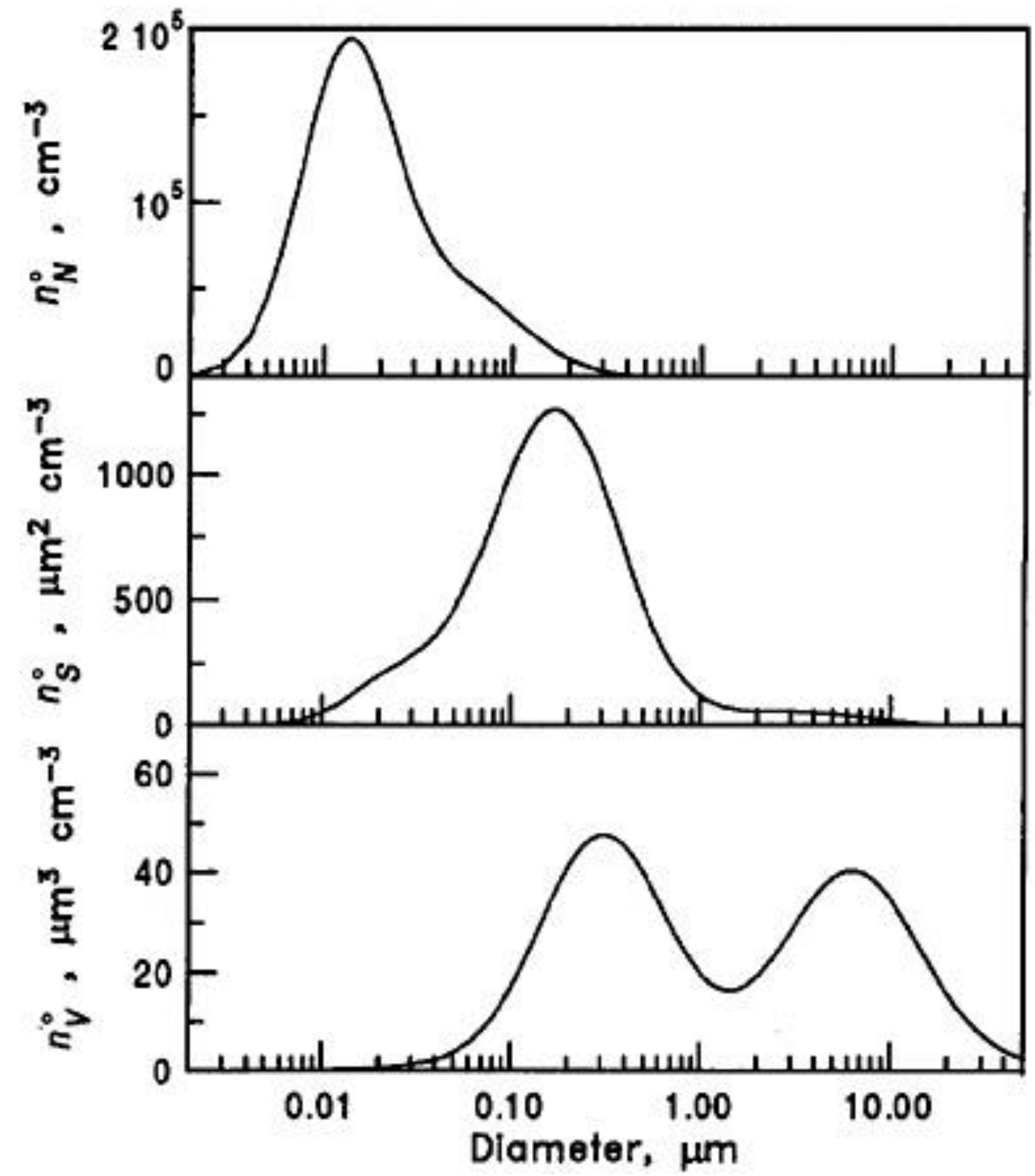

Figure 1.3.1 Particle volume (n°_V), surface area (n°_S), and number (n°_N) concentrations of urban aerosol as a function of particle diameter (Seinfeld and Pandis 2016).

The regulatory practice of reporting PM in terms of mass concentration has been called into question. It is common knowledge that the mass of small particles is negligible in comparison to the larger ones and, fine particulate matter has more negative health implications (Tuch et al. 1997). Furthermore regulatory agencies report PM concentration after it has been averaged over one day or even a year in some cases. Aerosol concentration and potential exposure can vary significantly within this time frame. Real-time measurements of number concentration would likely provide a more accurate depiction of particulate matter levels in a given area. One of the most widely used instruments for measuring number concentration of particles is the condensation particle counter (CPC). CPC's count the number of particles in an aerosol sample using a laser photodetector. However, most aerosol particles are less than 1nm in diameter, making them too small for the laser to see. A CPC overcomes this by condensing a working fluid such as alcohol, butanol, or ethylene glycol onto the surface of the particle until it grows to visible size. The type of working fluid is the primary difference between CPCs. The ability of the liquid to condense onto the surface of the particle is a mass transfer process that is driven by the molecular properties of the fluid. These differences in molecular properties lead to different counting efficiencies and minimum particle detection sizes.

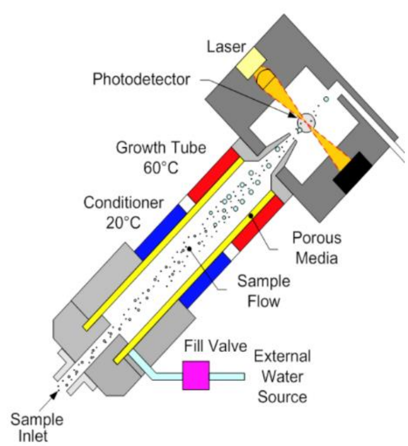

Figure 1.3.2 Basic Water CPC Schematic (TSI)

Several previous studies have been done in the comparison of different CPCs. For example, in 2017, a Finnish research group published a paper which examined the counting efficiency of three CPC's, each having different working fluids and the ability to detect particles less than 3 nanometers (Kangasluoma et al. 2017). The working fluids used by the instruments were butanol, water, and ethylene glycol. The researchers found that the water and ethylene glycol CPC's had very similar counting efficiencies while the butanol was significantly lower (Kangasluoma et al. 2017). They also compared the real-time particle counts of the water and ethylene glycol CPCs by taking measurements near a local bus stop (Kangasluoma et al. 2017). An earlier study compared the detection of sub 2nm in ultrafine CPC's that used non-hazardous, low volatility, working fluids such as ethylene glycol, oleic acid, diethylene glycol, propylene glycol, and diocytl sebacate (DOS) (Iida, Stolzenburg, and McMurry 2009). The results showed that the low vapor pressure of these fluids resulted in the aerosol particles growing sizes too small for the laser within the instrument to detect (Iida, Stolzenburg, and McMurry 2009). Thus, a second CPC was added to nucleate the particles to a detectable size and then examine the counting efficiencies (Iida, Stolzenburg, and McMurry 2009).

1.4 Overview of thesis

1.4.1 Objective

In the first half of this thesis we will discuss the physical characteristics of atmospheric aerosols and compare the different methods available for measuring them. One of these comparisons involved taking three different generations of CPCs into the field and analyzing the differences in their particle detection capabilities. The working fluids used in these CPC's were butanol and water. The CPCs are the TSI model 3787 Water, model 3772 Butanol, model 3776 Ultrafine Butanol, and the Teledyne model 651 Ultrafine water. In addition to our comparison of the different instruments and working fluids, we also compared our number concentration data to the mass concnetration data that is simultaneously reported by our the local regualtory agency, the

Maryland Department of the Environment (MDE). Since the size of particulate matter is of particular importance due to its implications on human and enviormental health, we also analyzed the particle size distribution of sampled particles and compared it to the concentration data that was collected simultaneoulsy. A comparison of this real time data allows us to better understand the size and levels of particulate matter that we could be exposed to.

While it is important to monitor the levels and size of particulate matter , it is also essential to monitor chemical compostion. The chemical nature is vital to detemirng the potential effects of an atmospheric aerosol. In part 2 of this thesis, we will discuss current chemical methods available for characterizing Black Carbon, an atmospheirc aerosol often classified as $PM_{2.5}$, and propose methods to conduct chemical measurements in real time.

1.4.2 Particle Sizing

While the CPC's determine particle number concentration, we rely on the Differential Mobility Analyzer (DMA) to determine the size of particles. The DMA relies on the premise that the electrical mobility of a single charged particle is a function of the particles size (Seinfeld and Pandis 2016). That is

$$B_e = qf(D_p) \tag{1.1}$$

where B_e is the electrical mobility and D_p is the particle diameter, and q is the particle charge. The function f (D_p) can be found through a force balance on a particle that has an external electric field applied to it. If an electric field is applied to a particle. The Summation of forces becomes,

$$\sum F = F_D - F_E \tag{1.2}$$

Where F is the total forces on the particle, F_E is the force of the electric field, and F_D is the drag force on the particle opposite the direction of the applied force. We assume the particle is at steady state and substitute the known forces (Seinfeld and Pandis 2016). By Stokes Law, the drag force becomes

$$F_D = \frac{3\pi\mu v D_p}{C} \tag{1.3}$$

where μ is the gas viscosity, v is the particle velocity, D_p is the particle diameter, and C is the Cunningham slip correction factor given by

$$C = 1 + \frac{2\lambda}{D_p}\left[\alpha + \beta * e^{\left(-\frac{\gamma D_p}{2\lambda}\right)}\right] \tag{1.4}$$

where α=1.165, β=0.483, γ=0.997 and λ is the mean free path (Kim et al. 2005). The Cunningham correction factor is an empirical fit applied to smaller particles due to their ability to slip through the space between molecules (Kulkarni, Baron, and Willeke 2011). This ability leads to higher velocities and reduced drag compared to what is normally predicted by stokes law(Kulkarni, Baron, and Willeke 2011). The addition of the Cunningham Correction factor accounts for this difference. The constants within the correction factor equation are dependent on the type of gas and its mean free path (Kulkarni, Baron, and Willeke 2011). The given values are for air when λ is 65nm.

The electric field force is given by

$$F_E = qE \tag{1.5}$$

where E is the strength of the electric field. Thus equation 1.1 and 1.2 becomes

$$B_e = \frac{v}{E} = \frac{qC}{3\pi\mu D_p} \tag{1.6}$$

From here we can see the relationship between electric mobility and particle size. The DMA exploits this by first using a radioactive neutralizer to apply positive and negative charges to an aerosol as it enters the system. The particles, still poly-dispersed, then enter a concentric column with an electric field applied using a high voltage rod in the center of the annular space (TSI Incorporated 2016 & references therein). The particles then fall along the column according to their electrical mobility, and flow rates of the instrument (TSI Incorporated 2016 & references therein)**.** Particles of high and low electrical mobility precipitate towards the top and bottom of the column respectively (TSI Incorporated 2016 & references therein). The particles with a narrow range of mobility exit the bottom of the column as a monodispersed aerosol to be counted using the attached CPC.

1.4.3 Lab Measurements

Preliminary measurements were conducted in the laboratory before moving to the field locations of College Park, MD and Beltsville, MD. In these tests we compared the particle detection of aerosols of known (Ammonium Sulfate) and unknown (Room Air) composition. In both cases, the ultrafine butanol CPC detects the highest concentration of particles. This is as expected since the ultrafine CPC has the lowest minimum particle detection limit. Its concentration is higher because it is likely detecting a large amount of fine particulate matter. We also see that the butanol and water CPCs measure very similar concentrations in both cases. This suggests there is little to no difference in the amount of particles detected by each instrument for the two aerosols sampled.

Table 1.4.1 CPC Comparison

TSI Model No.	Working Fluid	Minimum Particle Detection Size (nm)	Sample Flow Rate (L/min)
3785	Water	5	1
3787	Water	7	0.6 or 1.5
3772	Butanol	10	1
3776	Butanol	2.5	0.3 or 1.5

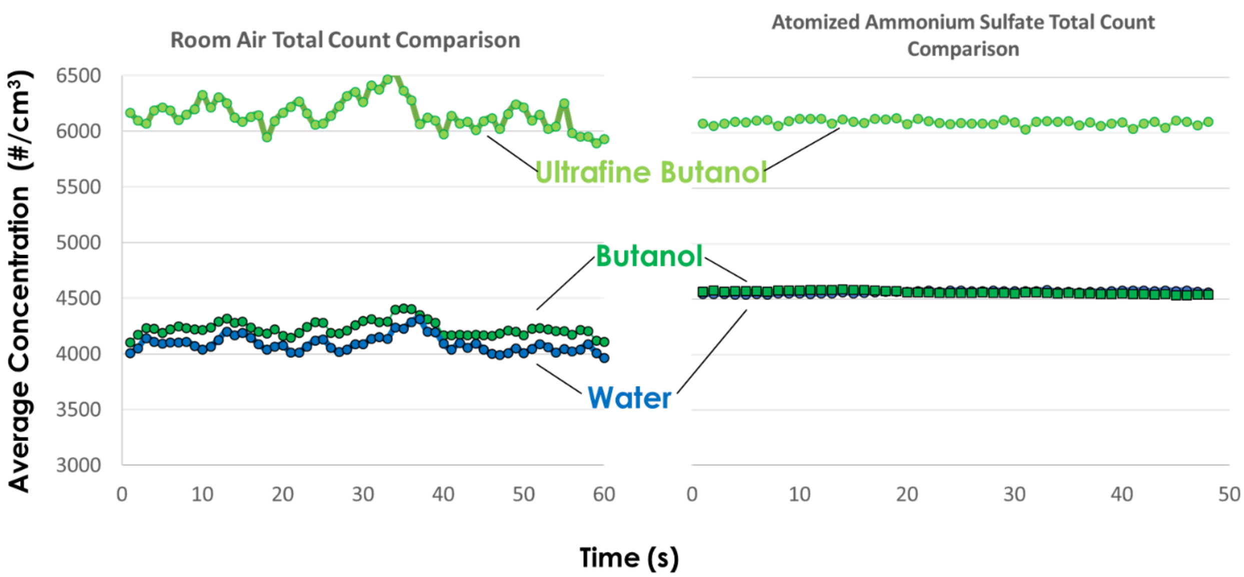

Figure 1.4.1 Average Particle Concentration from Room Air (left) and Atomized Ammonium Sulfate (right)

After comparing Total Counts, size comparisons were conducted in the lab using the DMA with the 3772 Butanol and 3785 Water CPCs. Black Carbon was the chosen aerosol due to its significance as a contributor to atmospheric $PM_{2.5}$ and its unknown size distribution. Figure 1.4 gives a comparison of the particle size distribution collected from the two instruments. We see that the particle concentration for the water CPC is about the same as the butanol at small particle sizes. However after about 50nm the agreement stops and the difference in particle count increase drastically. This is likely due to the interaction between the molecules. Water is polar and unable to completely condense onto the surface of the nonpolar soot particles. Conversely, butanol has a nonpolar end that is able to interact with the inorganic molecules of black carbon and condense onto its surface. However, the fact that at low diameters, the two instruments count the same number of particles lets us know that regardless of the working fluid properties, there can be agreement on particle number concentration at certain sizes. These findings were kept in mind when examining the size distributions of particles in the field.

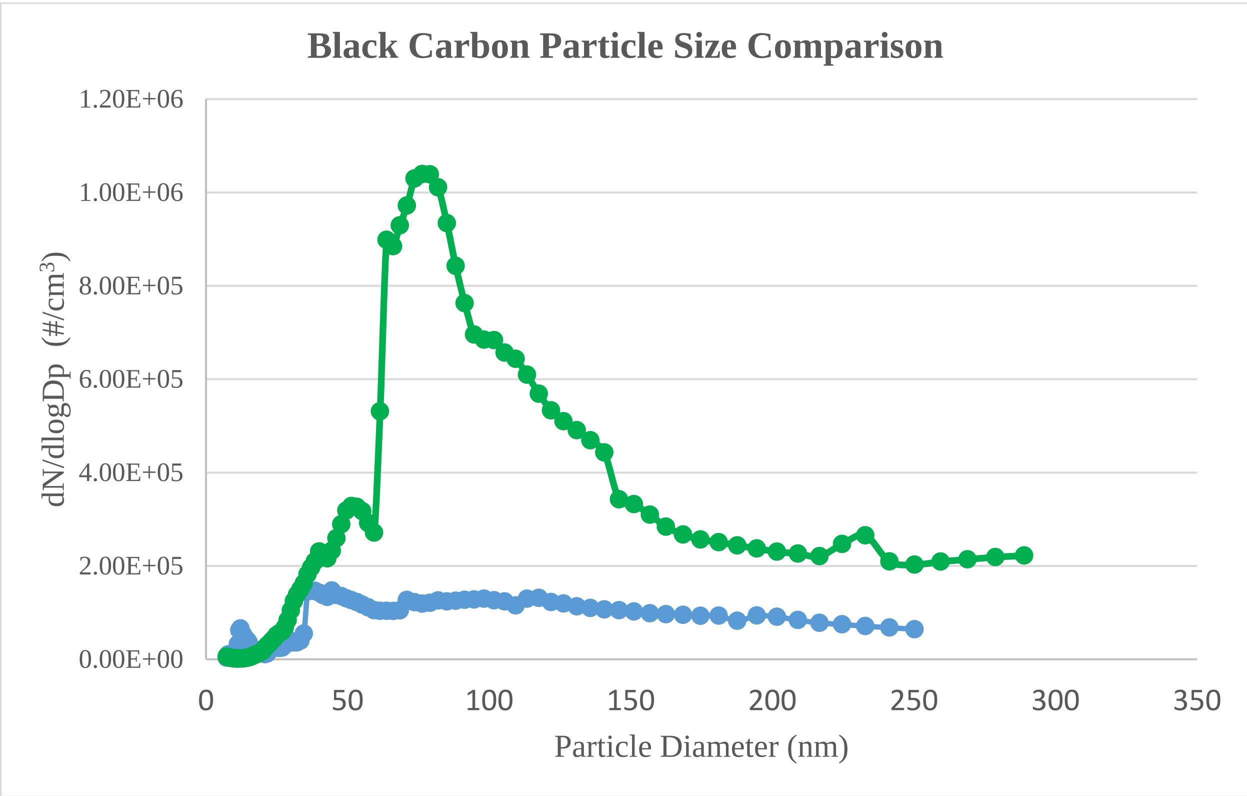

Figure 1.4.2 Butanol vs. Water CPC Black Carbon Particle Sizing Comparison

Chapter 2: Field Measurements & Physical Aerosol Detection Measurements

2.1 Research Objectives

While the EPA sets standards for acceptable limits of particulate matter, local agencies such as the MDE are responsible for monitoring particulate matter pollution levels and reporting when an area is not in compliance. The MDE has 25 air monitoring locations with the majority located in industrial and densely populated areas (Users et al. 2018). With roughly one station per county, they are equipped with instruments to measure the concentration of air pollutants and report regional air quality using the Air Quality Index ("Ambient Air Monitoring Network" n.d.). However, some of these counties are large and have varying topography and population density.

Figure 2.1.1 Map of Air Monitoring Stations in Maryland *(Users et al. 2018)*

Considering the nature of aerosols to travel throughout the atmosphere while participating in chemical and physical reactions, it is unlikely that the air sampled at one station provides an accurate description of the particulate matter concentration of an entire county. For example, Prince Georges County is the states 2nd most populated region. It is comprised of urban/industrial areas in the center and more rural areas to the north and south. Two locations are responsible for reporting air pollutant concentration in this county. The first is located in the rural southern region at the Prince George's Equestrian Center in Upper Marlboro, MD. According to the MDE, the scarcely populated area allows for the residential exposure levels of $PM_{2.5}$ to be monitored. The other location is the Howard-University Beltsville campus in Beltsville, MD. This is a more residential area and was chosen to measure $PM_{2.5}$ concentration at urban levels. However, figures 2.1.2 and 2.1.3 show that the locations appear to be similar with both showing residential development and a large area of vegetation.

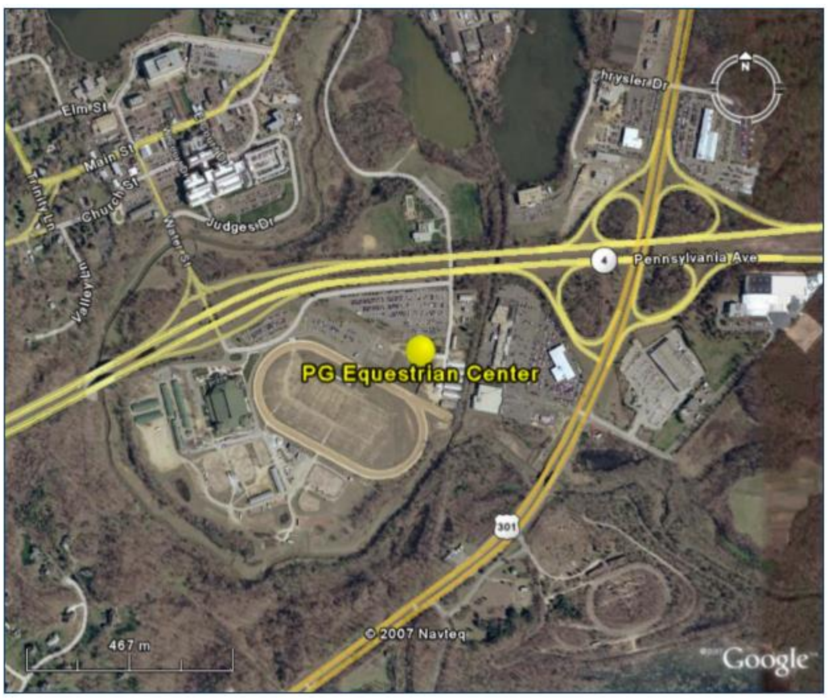

Figure 2.1.2 Satellite View of PG Equestrian Center Air Monitoring Station *(Users et al. 2018)*

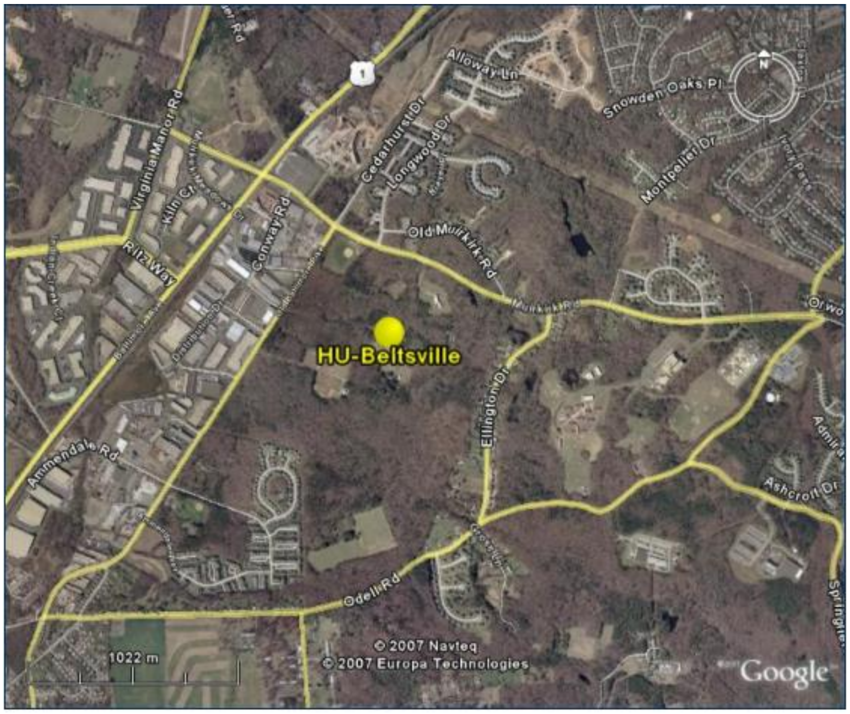

Figure 2.1.3 Satellite View of HU-Beltsville Air Monitoring Station *(Users et al. 2018)*

While the PG equestrian center may give an accurate particulate matter concentration for the rural, southern region of Prince Georges County, the HU-Beltsville site seems less likely to provide particulate matter information that represents the region. Figure 2.5 shows that the University of Maryland College Park campus is conveniently located less than 6 miles from the HU-Beltsville Monitoring Site. With the increased population and emission sources located on campus, it seems unlikely that the regional concentrations reported by MDE from the HU-Beltsville site would accurately describe particle concentration in this area. This begs the question, do the local concentrations of particulate matter vary significantly from the regional values reported by the MDE? Furthermore, the concentrations that are reported are done in terms of mass. If there is any agreement between the two measurement locations in terms of number concentration, will there be a correlation between the mass and number concentration of the particulate matter?

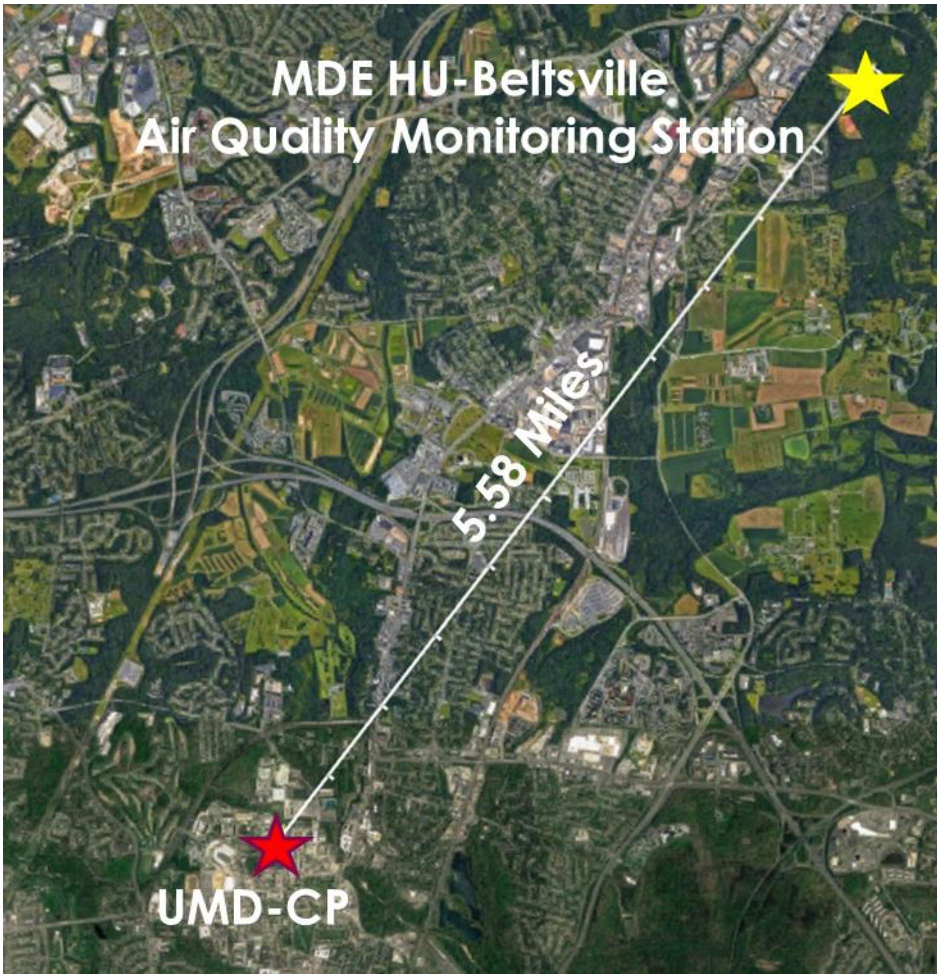

Figure 2.1.4 Distance between College Park and HU-Beltsville Sampling Locations

2.2 Methodology

In order to determine if there was any variability in local and regional concentrations, we first had to make sure that the data from our instruments was comparable to the data gathered by the CPC at the HU-Beltsville site. The TSI 3776 Ultrafine Butanol and TSI 3772 Butanol CPC's were taken to the site to be run simultaneously with MDE's Teledyne 651 Ultrafine Water CPC. Tygon tubing was connected from the inlet of all three instruments to a four-way connector. The connector was then fitted to a void volume with the other side open to the ambient air. The void volume is added to mitigate the variations in data collection that might be caused by the differences in the instruments flowrates. The TSI 3776 Ultrafine butanol has an inlet flow of 1.5 liters per minute while the TSI 3772 Butanol pulls in aerosols at a rate of 1 liter per minute (LPM). The inlet flow rate of the Teledyne 651 Ultrafine Water CPC is substantially higher at 3.0 liters per minute. This larger flowrate could likely have had an effect on the inlet pressure of the other two CPC's. Thus, Teledyne's inlet line was made to be slightly longer than those of the other two instruments.

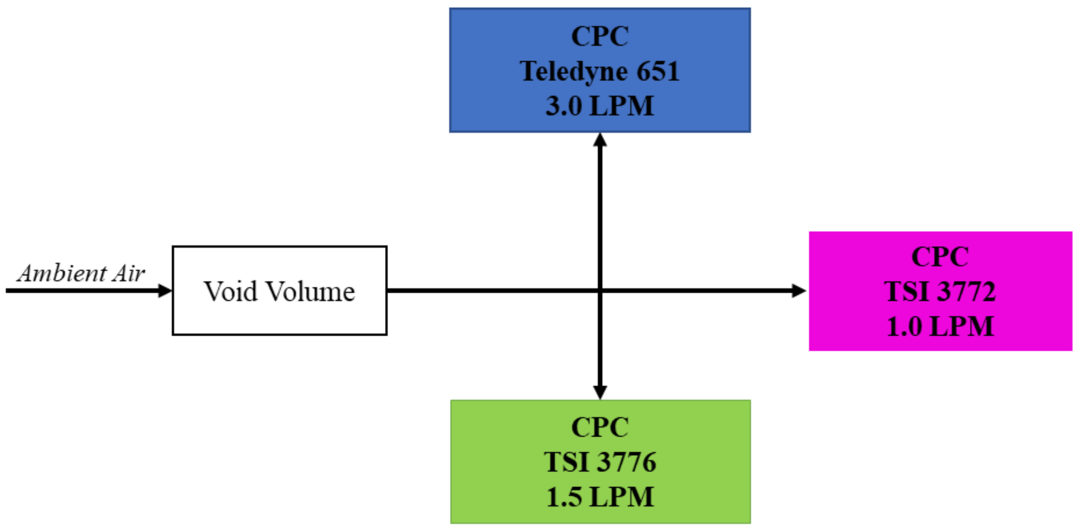

Figure 2.2.1 CPC Sampling Flow Schematic

The instruments were installed and allowed to sample for 5 days gathering time series data regarding the number concentration of the particles. The TSI CPCs collect particle data every second and the Teledyne CPC's average over 5 seconds. All instruments have a 1 hour sampling time. In addition to particle count, we were also interested in the size of particles. This required the use of the DMA in conjunction with TSI 3772 CPC. As particles are scanned according to their electrical mobility by the DMA, they are counted by TSI 3772 Butanol CPC. The use of the TSI 3772 Butanol CPC with the DMA means no concentration data could be collected and only the

Teledyne 651 Ultrafine Water and TSI 3776 Ultrafine Butanol could collect concentration data for comparison. Particle size data was collected for roughly 30 hours and compared with the concentration data provided by the CPCs in order to determine how particle count varies with size distribution over this specific range of time.

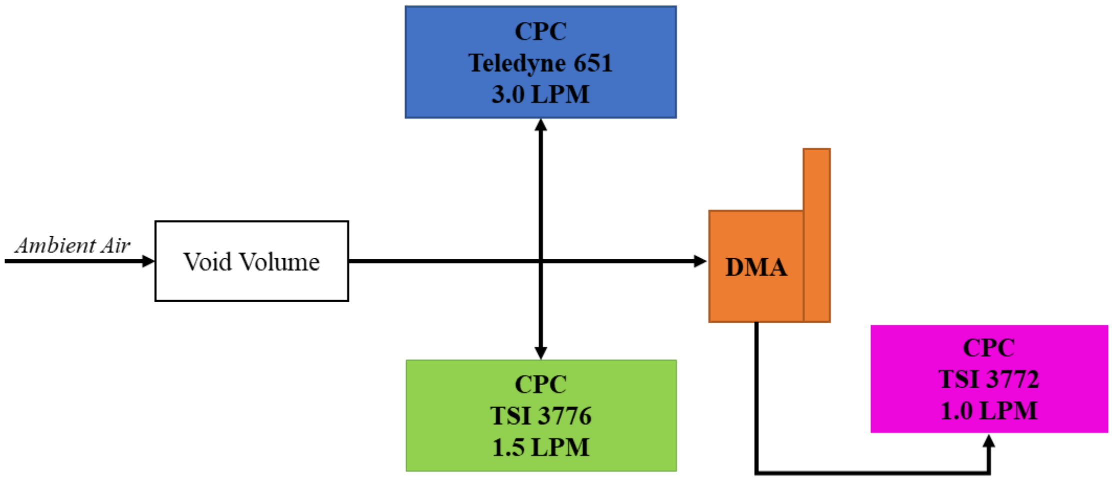

Figure 2.2.2 HU-Beltsville CPC Sampling Flow Schematic with DMA attached

Once it was established that the MDE instrument and our own CPC's had comparable number concentration, the instruments were returned to college park for ambient measurements. These measurements are then compared to the regional values reported by the MDE Teledyne Ultrafine Water CPC. The sampling at college park took place in the closed rooftop lab of the Atmospheric and Oceanic Sciences Department at the University of Maryland College Park. In comparison to the HU-Beltsville site which is located in the middle of a field, the College park sampling site is located in the middle of a busy university campus with continuous exposure to emission sources. The facility is adjacent to a bus stop, parking garage, and an on-campus farm. It is also situated on a rooftop roughly 130 foot above the ground. This will allow for a better mixed aerosol concentration in comparison to the 10 feet sampling height of the HU-Beltsville site. The TSI 3776 Ultrafine Butanol, TSI 3787 Water, and TSI 3772 Butanol CPC's were used for all sampling at this facility. Similarly to the Beltsville site, Tygon tubing was used to connect the inlet of each instrument to a 4-way connector which was subsequently attached to a void volume. Again this was done to mitigate the difference in flow rates (TSI 3787 Water has an inlet flow of 1.6 LPM). Once all three instruments are connected to the void volume, a line from outside the facility is connected to the void volume allowing all three CPC's to pull directly from ambient air. The instruments were set to collect concentration data over a period of 5 days similarly and Particle size data was also collected for a period of roughly 30 hours. However, unlike the HU-Beltsville run, two identical TSI 3772 Butanol CPCs were available. One was used to monitor particle counts while the other was used in conjunction with the DMA to measure particle size distribution.

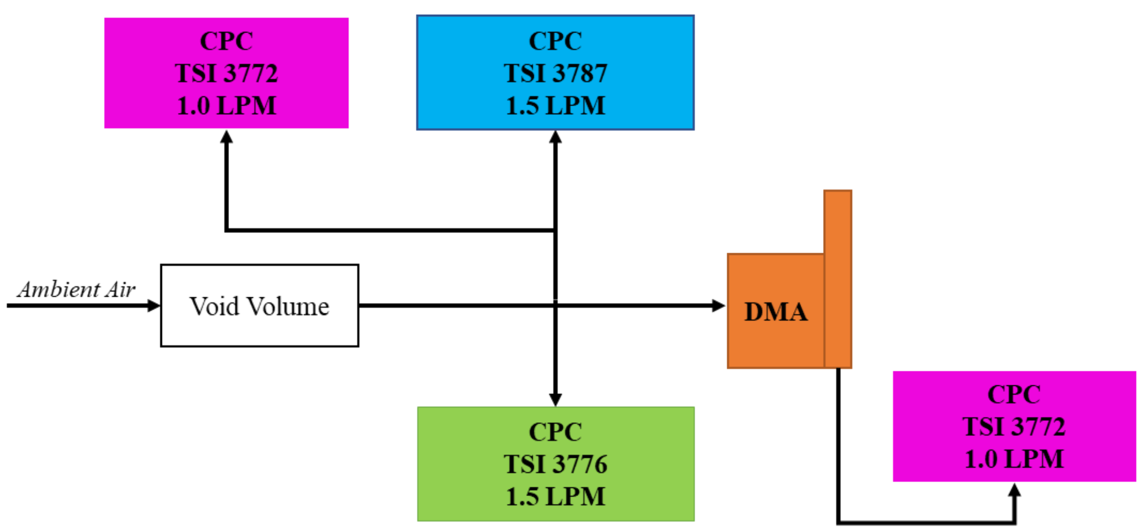

Figure 2.2.3 CPC College Park CPC Flow Schematic with DMA Attached

2.3 Results

The total particle concentration measured at both locations mirrored what was seen in the lab. In both cases, the TSI 3776 Ultrafine Butanol CPC counts the highest number of particles, followed by the TSI 3772 Butanol, and either the Teledyne 651 Ultrafine Water CPC at the HU-Beltsville site or, the TSI 3787 Water CPC at the College Park site. Figure 2.3.1 shows how the TSI butanol CPC's compare to the MDE's Teledyne 651 Ultrafine Water CPC when measurements are taken at MDE. Figure 2.3.2 compares all of the TSI CPC measurements at the College Park sampling site to data that was simultaneously gathered at the HU-Beltsville site. In all measurements, the number of particles measured by the Teledyne 651 Water CPC are comparable to those of the other instruments and indicate that the MDE's reported concentration are generally accurate representations of particle concentration in the region. However, further data analysis is required to verify this.

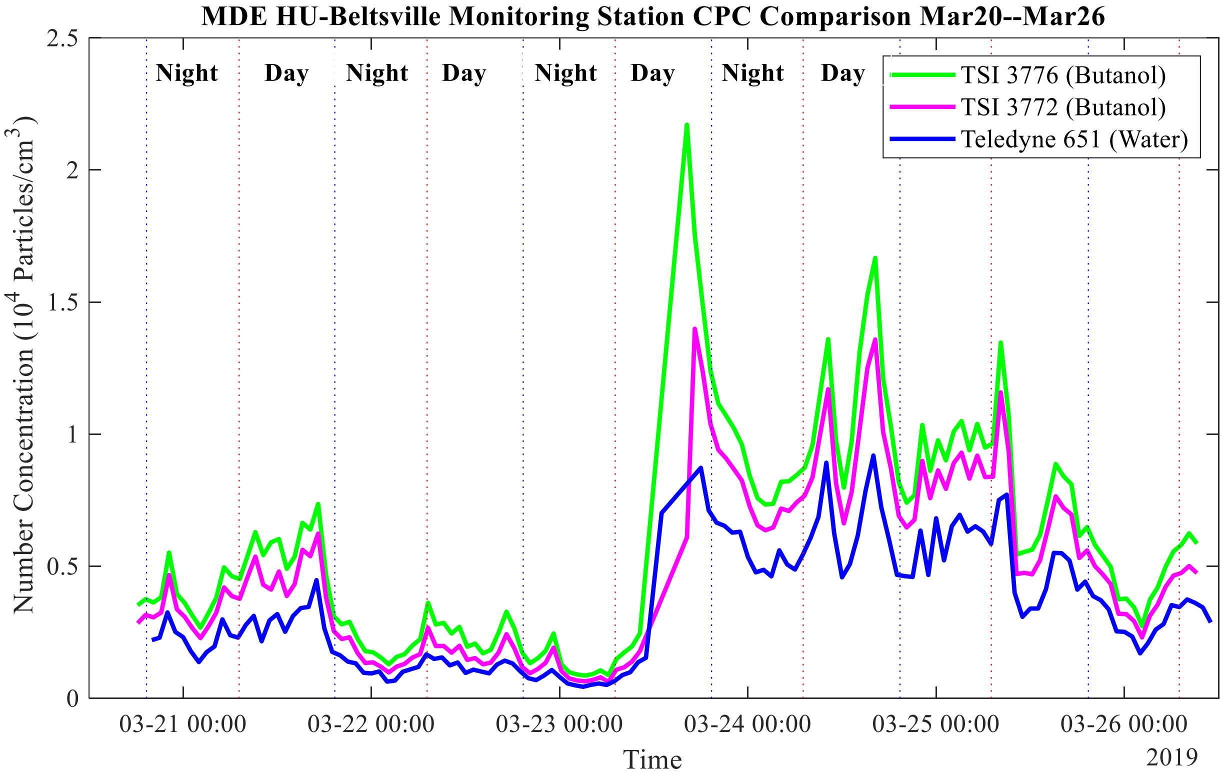

Figure 2.3.1 CPC Particle Count Comparison from HU-Beltsville Monitoring Station

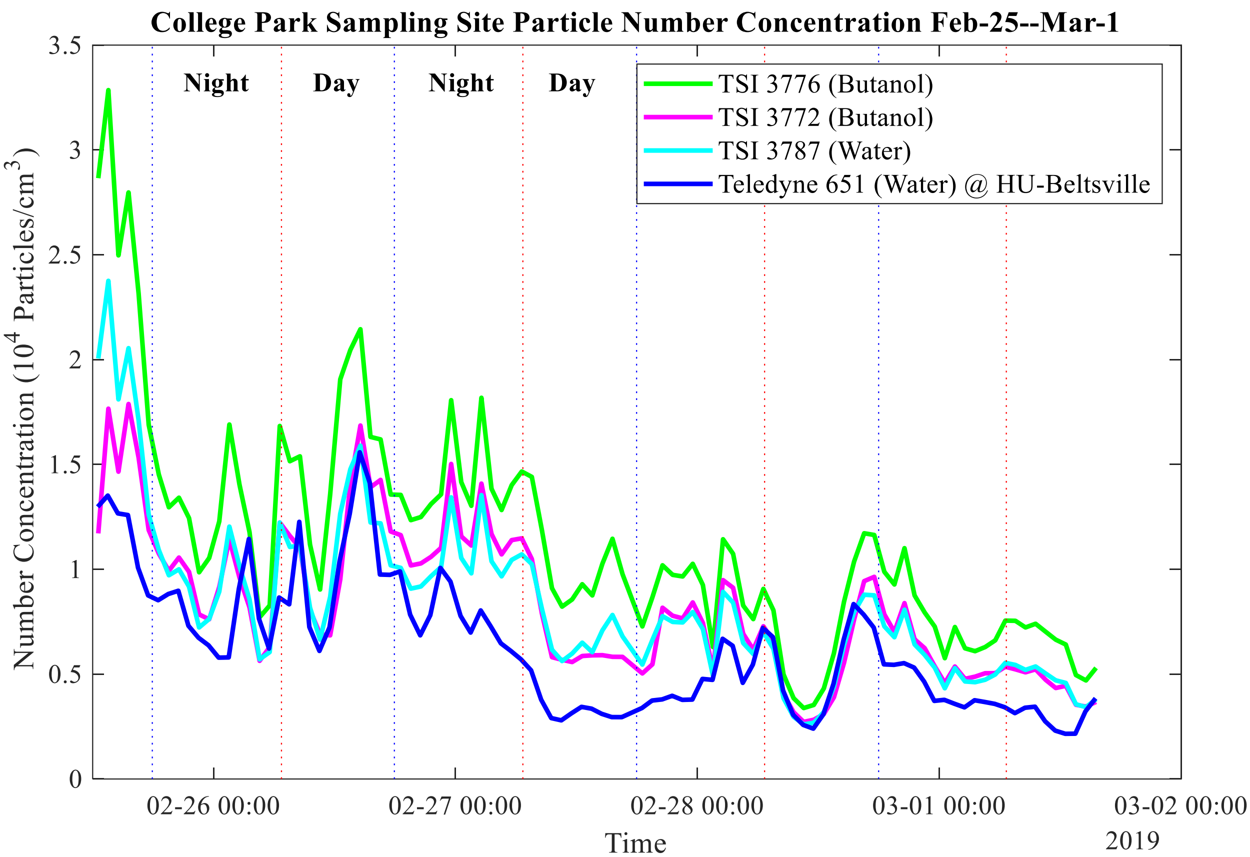

Figure 2.3.2 CPC Particle Count Comparison from College Park Monitoring Station with Simultaneous with Simultaneous Measurements from HU-Beltsville

Particle Size distribution data was collected for a short portion of time at both measurement locations. Figure 2.3.3 shows how the size distribution of the particles at the College Park site varied over the first 30 hours of sampling. These distributions can be matched to the concentration data displayed in Figure 2.3.2 for the same time frame. Figure 2.3.4 reflects the particle size distribution for another 30 hours sampling ambient air. However this was done at the HU-Beltsville monitoring station. Figure 2.3.5 gives the concentration data that corresponds to this time. In the sample from the College park site, we see a smaller range of particle sizes in comparison to the HU-Beltsville site. Furthermore, the College Park Site exhibits maximum concentrations of

~50,000 particles per cubic centimeter in the early samples, at low diameters. However, the MDE the maximum concentrations reached are ~20,000 particles per cubic centimeter and occur at larger diameters.

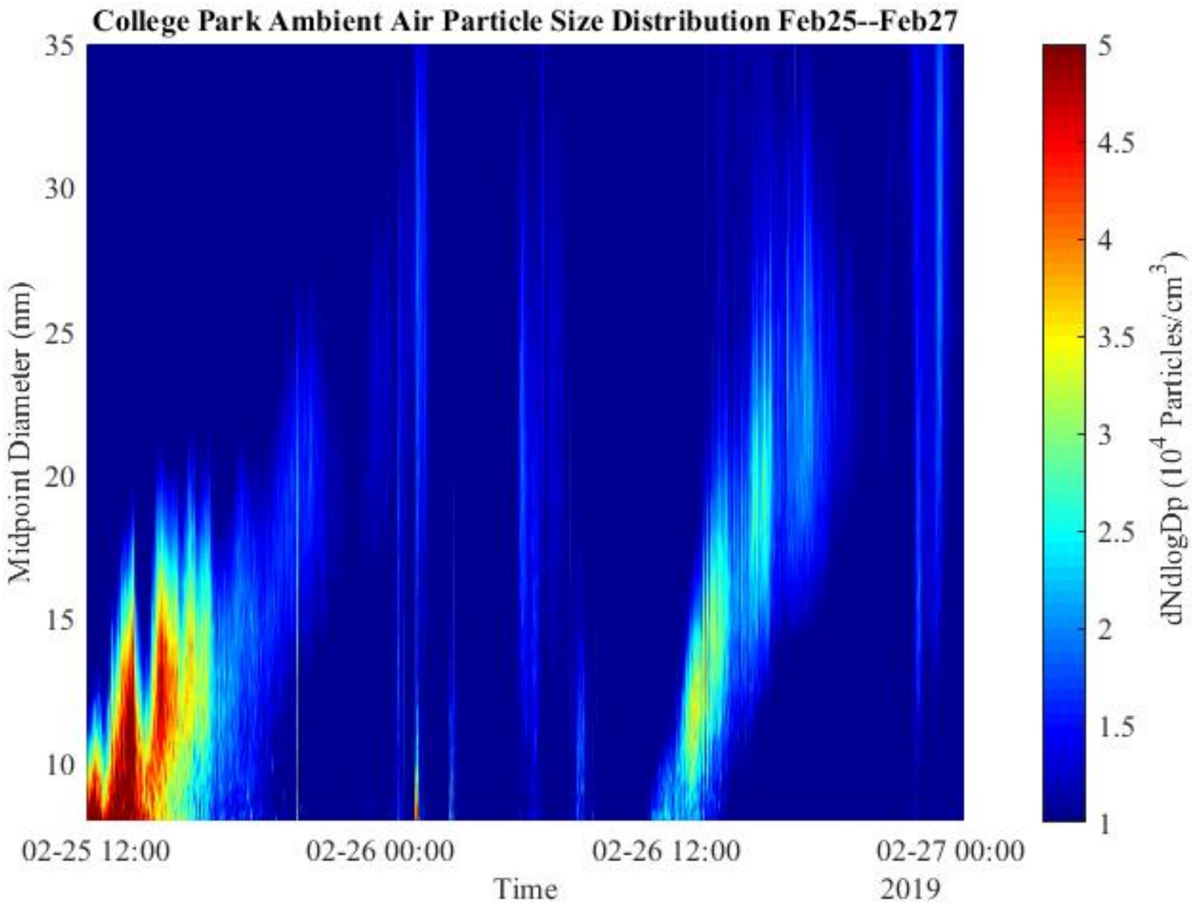

Figure 2.3.3 Particle Size Distribution Time Series from College Park Sampling

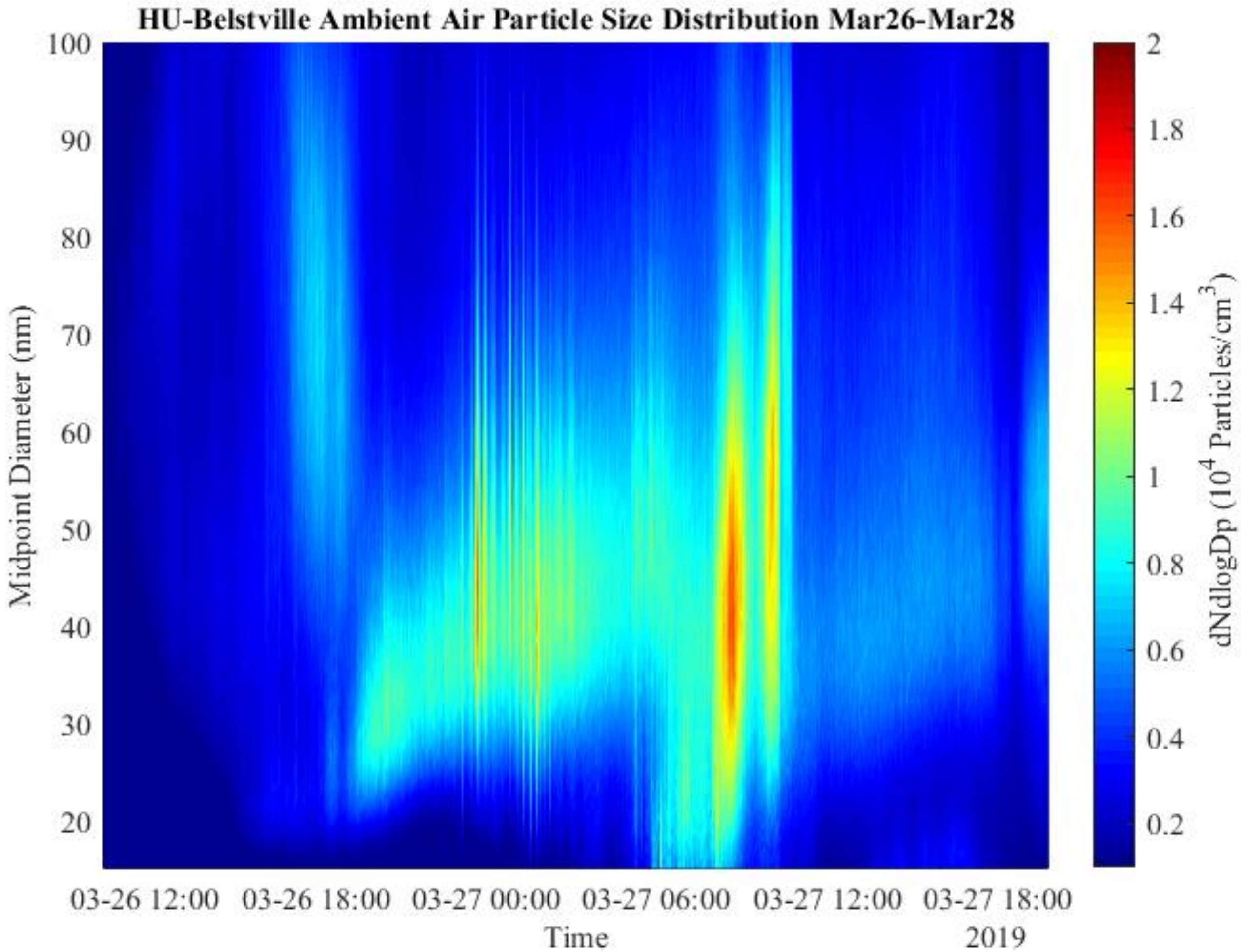

Figure 2.3.4 Particle Size Distribution Time Series from HU-Beltsville Sampling

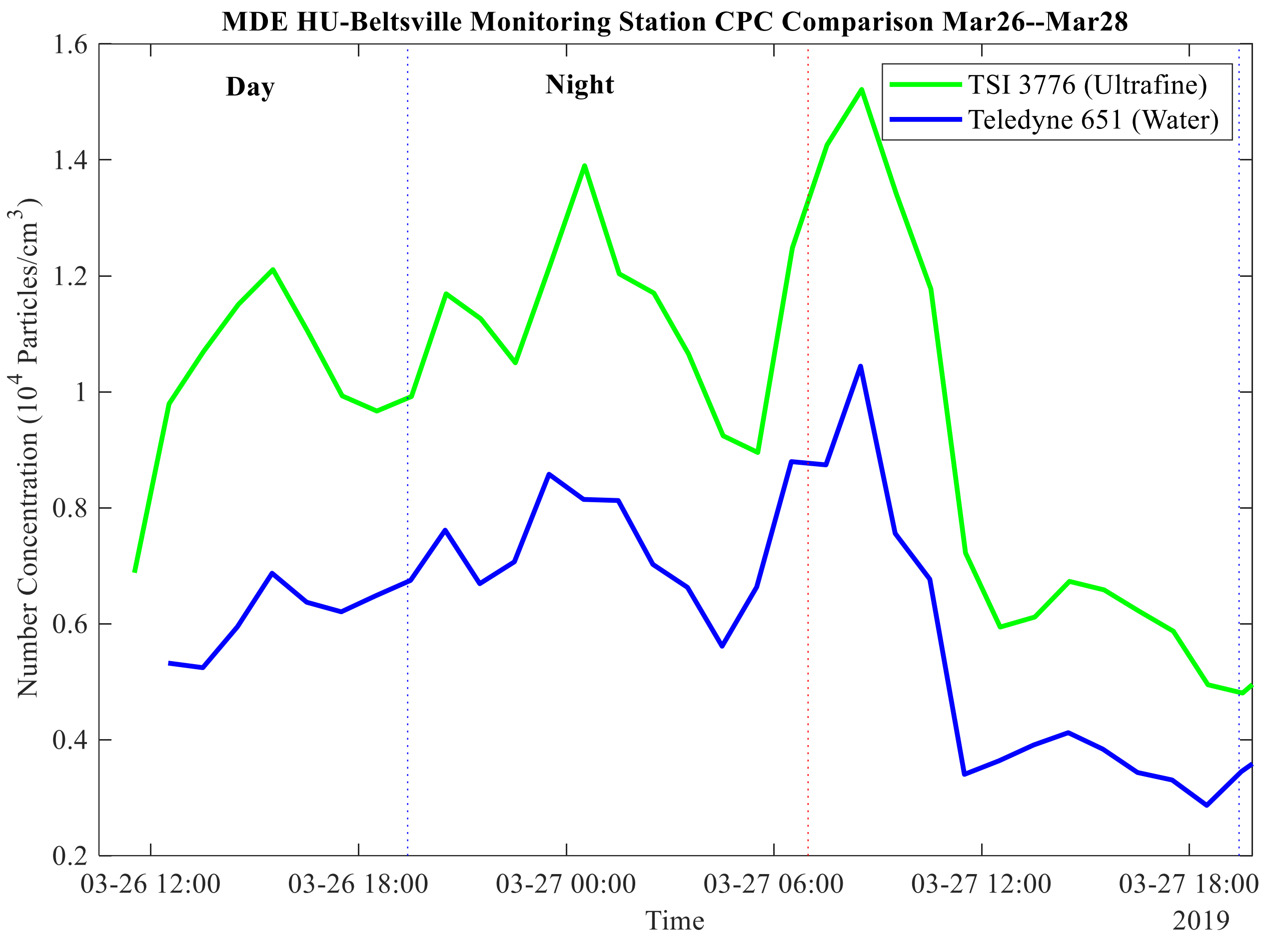

Figure 2.3.5 CPC Particle Count Comparison from HU-Beltsville Monitoring Station during Particle Size Distribution Sampling

2.4 Discussion

When comparing the measurements taken at the MDE's HU-Beltsville facility on a one-to-one plot, the trends observed in the lab appear to hold. Figure 2.4.1 compares measurements taken using the TSI 3776 Ultrafine Butanol and the TSI 3772 Butanol CPC's. Here, we see that while the 3772 is undercounting in comparison to the 3776, the difference is mostly within 10-25% and the relationship is linear. The difference between the two ultrafine CPC's is less linear in nature. Figure 2.4.2 shows the one-to-one relationship of the two instruments simultaneous measurements. The trend of water CPCs undercounting the Ultrafine Butanol still holds. However, the difference in concentration between the two instruments is larger. The majority of the Teledyne measurements undercount the TSI 3776 by 10-50%. Furthermore, a sizeable portion of the measurements from the Teledyne undercount the TSI 3776 by greater than 50%.

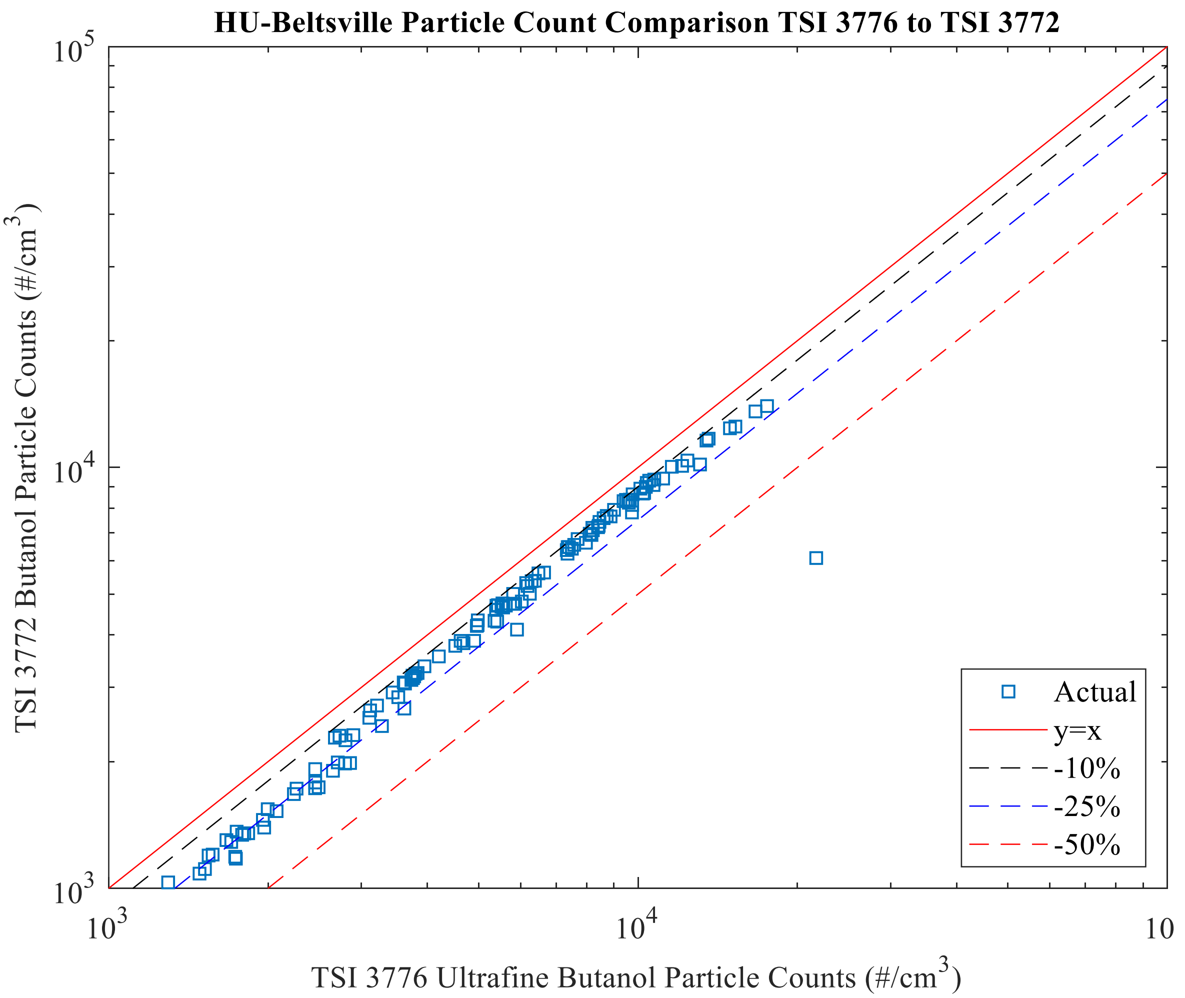

Figure 2.4.1 One-to-One CPC Particle Count Comparison of TSI 3776 and TSI 3772 at from HU-Beltsville Monitoring Station

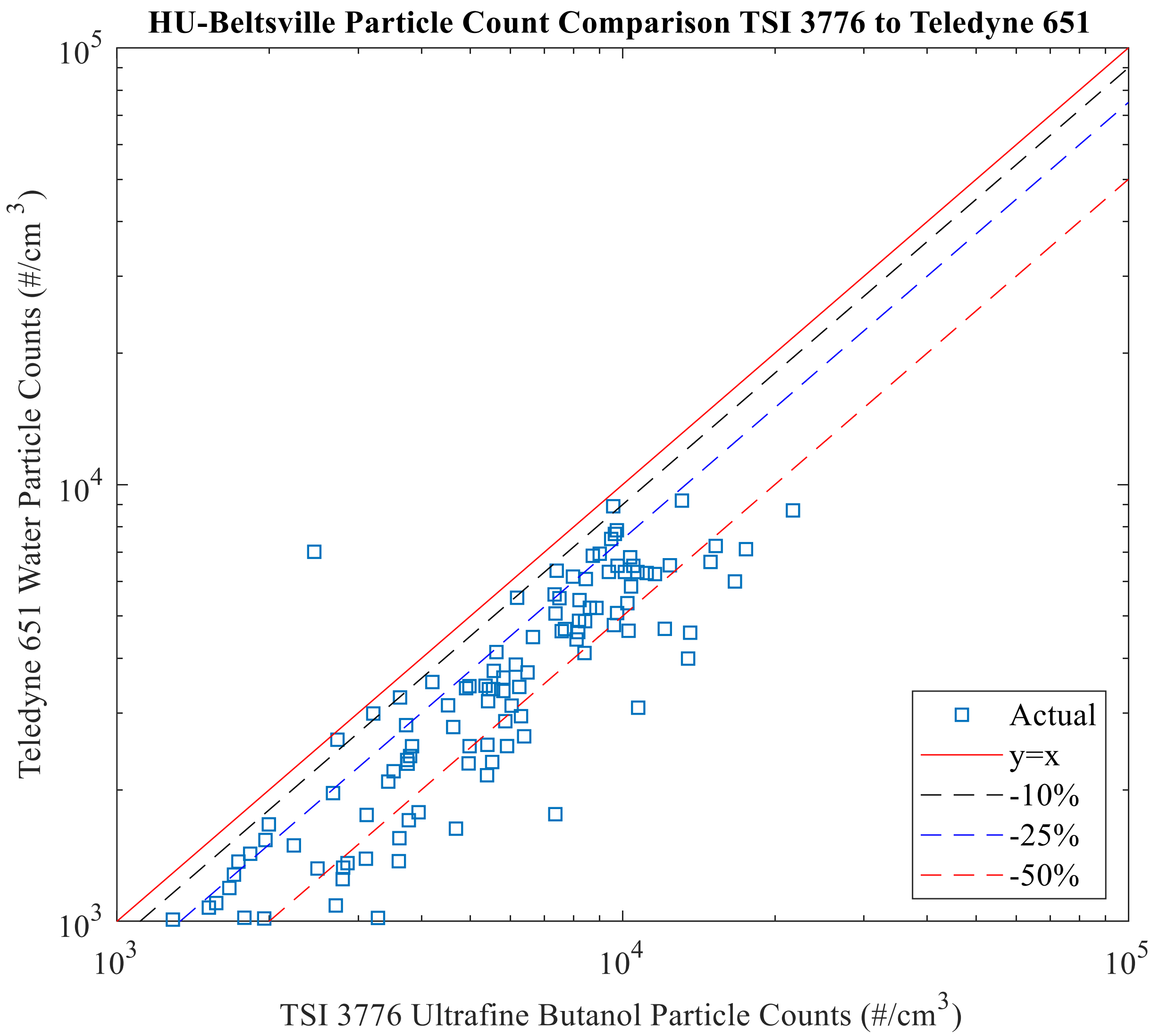

Figure 2.4.2 One-to-One CPC Particle Count Comparison of TSI 3776 and Teledyne 651 at from HU-Beltsville Monitoring Station

In order to determine if there is substantial variation in the particle measurements of the two locations, we need to compare data in Figure 2.4.2 to the data set that contains measurements taken at the College Park facility and simultaneous concentrations reported by the MDE from the HU-Beltsville site. By linearizing the two data sets and comparing the slopes, we can determine if there is substantial variation between the instruments at different locations.

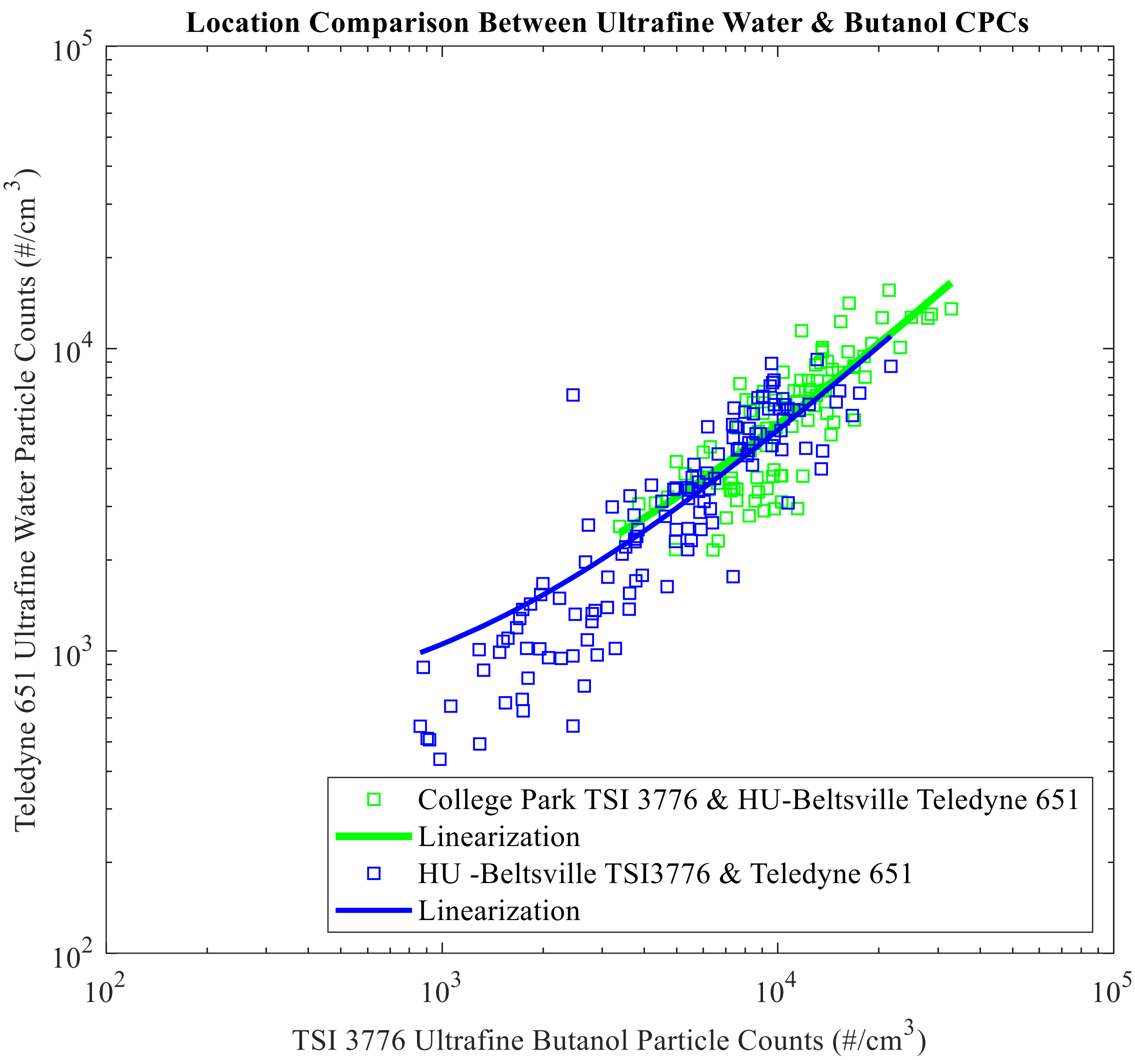

Figure 2.4.3 One-to-One CPC Particle Count Comparison of TSI 3776 and Teledyne 651 at College Park and Beltsville Locations

The linear relationship between the data collected at the College Park Site and the data from the HU-Beltsville air monitoring station is described by the equation 2.1 where *x* is the number concentration reported by the TSI 3776 Ultrafine Butanol CPC and *y* is the corresponding concentration reported by the MDE at the HU-Beltsville site using the Teledyne 651 Ultrafine Water CPC.

$$y = 0.4767x + 844.0925 \tag{2.1}$$

When both instruments sample at the HU-Beltsville site, the equation becomes

$$y = 0.4795x + 572.8278 \tag{2.2}$$

The difference in of the two slopes in equations 2.1 and 2.2 is 0.6%. This indicates that the two slopes are nearly identical and the relationship between the Number of Particles counted by the TSI 3776 Ultrafine Butanol CPC and the number counted Teledyne 651 Ultrafine water CPC is independent of the location of the TSI CPC. The measurements were conducted on different days at different locations, yet the slope is still the same. While it has been established that the number concentration data reported by the MDE at the HU-Beltsville site may undercount the data recorded by the TSI instruments, there appears to be little to no variation between the two locations tested here.

In addition to our study of the relationship between number studies, we are also interested in comparing our measured numbered concentrations to the mass concentrations of $PM_{2.5}$ reported by the MDE. Figure 2.4.4 replots the concentration data from the HU-Beltsville facility (Figure 2.3.1) and adds the average hourly mass concentration of $PM_{2.5}$ as reported by the MDE from the HU-Beltsville site. Upon visual examination, it does not appear that any relationship exists between the $PM_{2.5}$ and any other data set. Another one-to-one plot is constructed to analyze verify this. Figure 2.4.5 compares the $PM_{2.5}$ mass concentration to the TSI 3776 Ultrafine Butanol number concentration. Here we see that there seems to be no correlation between the data sets. An attempt at linearization produces an R^2 value 0f 0.0042.

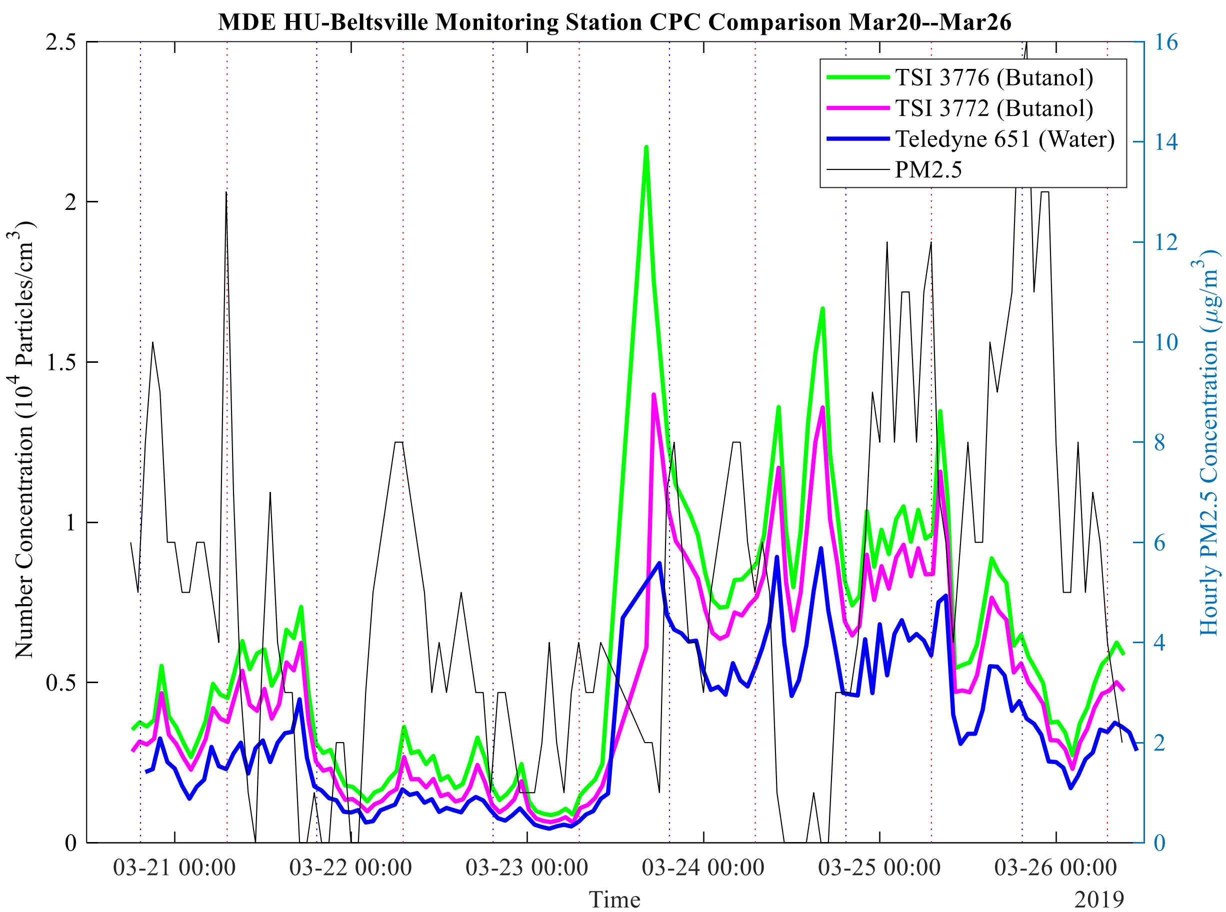

Figure 2.4.4 CPC Particle Count Comparison from HU-Beltsville Monitoring Station with $PM_{2.5}$ mass concentrations reported by the MDE

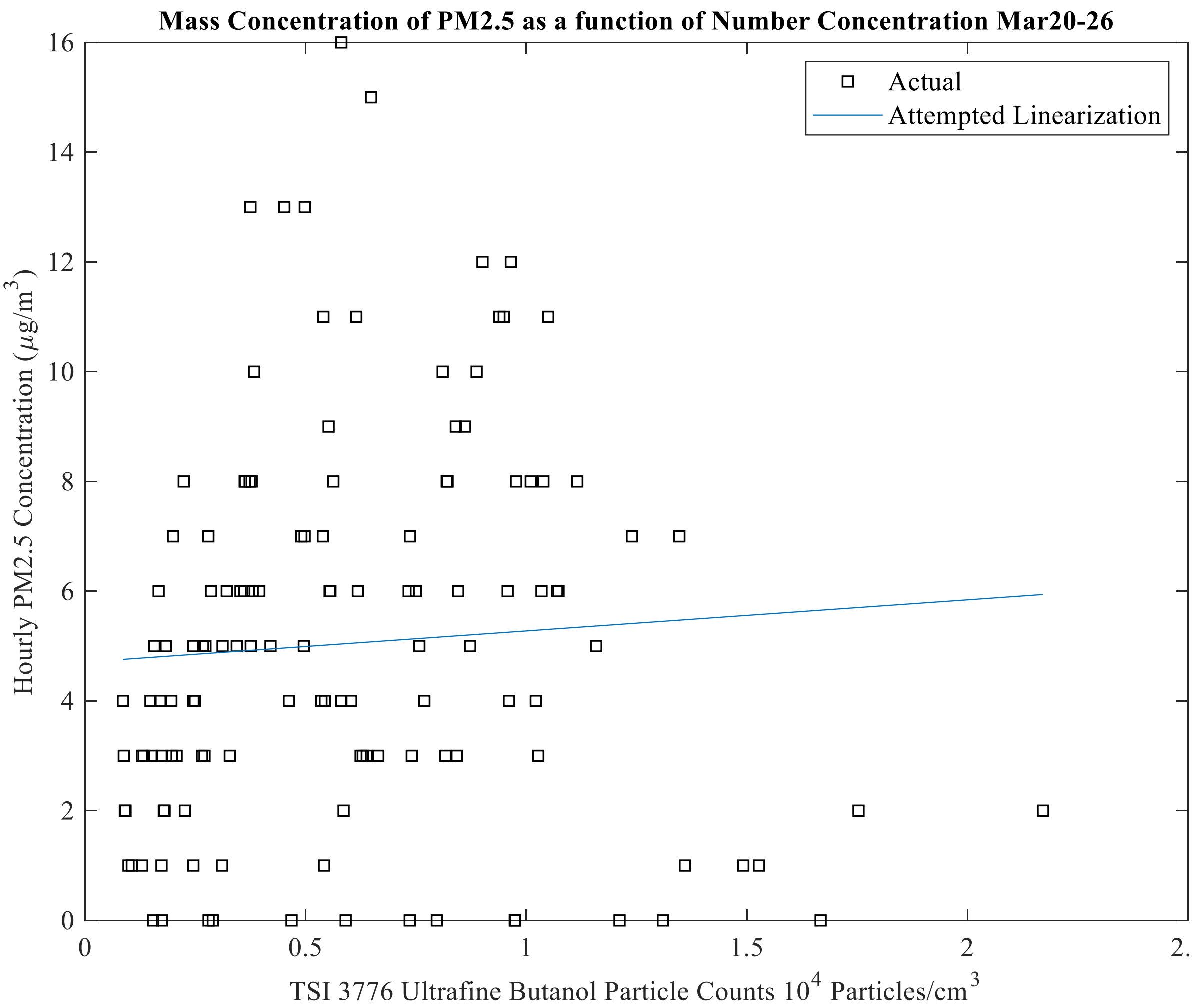

Figure 2.4.5 Hourly $PM_{2.5}$ mass concentration at HU-Beltsville as a function TSI 3776 Ultrafine Butanol CPC Number Concentration

Further examination of the particle size data given in Figures 2.3.3-2.3.5 give us some notion of the relationship between the sizes of the particles and there measured concentration. For instance in Figure 2.3.4, we see a decrease in particle number concentration between about 7 AM and noon on March 27th. During this same period, Figure 2.3.5 shows that there is a sharp increase in the concentration of particles between 30 and 50nm. This could be describing a nucleation event. Nucleation occurs when submicron aerosol particles cluster together and form large aerosol droplets. As smaller particles cluster together to form more particles, the concentration of larger particles increase, while the total number concentration of particles decrease. In the atmosphere, new particles are typically formed during the early morning hours and then nucleate throughout the day (Kulmala 2003). The increase in particle concentration we observe between 4 and 7AM could be the caused by the formation of new particles. This leads to nucleation events later on in the day that cause the total particle concentration to decrease. Observations over longer periods of time would be required to determine if this is the case here. Unfortunately, the size distribution data gathered was limited in comparison to the particle concentration data gathered over the course of this study.

2.5 Conclusion

Based on the results discussed thus far, it appears that there is little to no variation in aerosol number concentration between the MDE's HU-Beltsville facility and the College Park campus located roughly 5 miles away. This is slightly surprising considering the wealth of emission sources near and on the College Park campus and the location of the MDE- sampling site in an empty field near a residential area. However, this does suggest that the MDE Air monitoring station at HU-Beltsville is situated in a location where it can accurately report particulate matter levels for at least a 5 mile radius. In order to determine true extent of this Air Monitoring stations coverage, future studies should conduct field measurements at sites further from the HU-Beltsville site and compare them to MDE findings. In addition, any future studies should attempt to compare the mass concentrations reported by the MDE to other mass concentrations taken in the field. This study has shown that there is no correlation between mass concentration and rea-time number concentrations. Furthermore, future studies should also attempt to gather particle size data for the entirety of the sampling time. This will enable the robust comparison of size distributions to total particle counts, making it easier for nucleation events to be identified. Thus far, all the measurement techniques described in this chapter have been physical. However when dealing with atmospheric aerosols, physical properties hold equal importance to chemical properties. The number or mass concentration of an aerosol has much more meaning when we know its chemical composition. It is also easier to point out phenomena such as nucleation because we know which particles are more likely to participate in it. In the next chapter, we discuss the use a chemical technique known as Raman Spectroscopy and its use in the measurement of black carbon particulate matter.

Chapter 3: Chemical Characterization of Aerosol Particles Using Raman Spectroscopy

3.1 Overview

3.1.1 Black Carbon

Black Carbon (BC) is formed through the incomplete combustion of fossil fuels and biomass. These soot particles are graphitic in structure. Prior to modification in the atmosphere, they are comprised almost purely of carbon molecules, with negligible amounts of oxygen and hydrogen (Andreae and Gelencser 2006). BC is a class of carbonaceous material similar to elemental carbon (EC) and brown carbon (C_{brown}) (Andreae and Gelencser 2006; Lack et al. 2014). Elemental carbon is the defined as the carbonaceous material “thermally stable in an inert atmosphere up to 4000K” (Lack et al. 2014). This term is often misused in literature to imply a “ near-elemental soot-carbon-like composition” (Andreae and Gelencser 2006). C_{brown} is the light absorbing organic carbon in atmospheric aerosols of various sources (Andreae and Gelencser 2006; Lack et al. 2014). Often times in literature, the term “BC” is used to refer to all forms of light absorbing carbonaceous material. For the purposes of this chapter, we will define BC as the combustion byproducts described earlier.

In the United States, BC accounted for about 12% of the $PM_{2.5}$ emitted in 2005 (Hemby et al. 2012). This is the equivalent of roughly 1.7 million tons of BC emitted into the atmosphere in the U.S. alone (Hemby et al. 2012). BC is also associated with the negative health effects of $PM_{2.5}$ discussed in chapter 1, including respiratory and cardiovascular impairments. It is often emitted with other harmful pollutants such as benzene, formaldehyde, polycyclic organic matter (POM) and carcinogenic polycyclic aromatic hydrocarbons (PAHs) (Hemby et al. 2012).

Combating the emissions of BC and other light absorbing carbonaceous materials is made difficult due to their many sources. About 35% of global BC emissions are a result of biomass burnings (Hemby et al. 2012). Biomass is also burned in homes to produce heat for cooking. Over 2 billion people around the world use crude biofuels such as wood, coal, and refuse in inefficient, traditional stoves. making domestic sources the 2nd largest source of BC emissions (Legros et al. 2009; Hemby et al. 2012). In more industrialized nations such as the United States, over 50% of the BC emission comes from transportation sources (Hemby et al. 2012). Heavy duty commercial vehicles powered by diesel are some of the largest contributors of BC. BC also has significant environmental impacts. In chapter 1, it is mentioned that dark, light absorbing particles such as BC have a net positive radiative forcing on the atmosphere. Small changes in its concentration can lead to either positive or negative changes in radiative forcing (Haywood and Shine 1995). BC particles also deposit on snow and absorb solar radiation that would otherwise be reflected by the sun, leading to snow-melt and the rising of sea levels (Flanner et al. 2007). Light absorbing carbonaceous materials such as BC are the predominant light absorbing compounds in the atmosphere (Andreae and Gelencser 2006). Thus, monitoring the concentration of BC is essential to understanding radiative forcing and climate change (Madhavi Latha and Badarinath 2003).

3.1.2 Chemical Measurement Methods

With the many sources, health risks, and environmental threats associated with BC, it is essential to monitor the composition and number of BC aerosols. Several techniques exist to measure BC and other carbonaceous materials in the atmosphere. For example, an aethalometer can estimate atmospheric BC concentration by continuously measuring the light transmittance (at a wavelength of 880nm) rate of change in absorption light of particles deposited on a glass fiber filter. From this, it can estimate mass of the BC deposited (Phairuang et al. 2019). Using the light absorption aethalometer measurements at visible, ultraviolet, and infrared wavelengths, models that differentiate between the sources of BC can be developed (Sandradewi et al. 2008). Another technique is Multi Angle Absorption Photometry (MAAP). This method measures the radiation that is absorbed and scattered from a particle loaded fiber filter at different angles, and can be used to find the mass of BC particles (Andreas Petzold and Schönlinner 2004; Slowik et al. 2007). In another method, Photoacoustic Spectroscopy, particles are irradiated using a laser source causing an increase in acoustic pressure (Slowik et al. 2007; Patrick Arnott et al. 1999). The acoustic pressure is then used to calculate the aerosol absorption coefficient and mass concentration of BC (Slowik et al. 2007; Patrick Arnott et al. 1999). Infrared spectroscopy, specifically Fourier Transform Infrared Spectroscopy (FTIR) has also been used in the characterization of BC particles. In this process, particulate matter is gravimetrically sampled onto polytetrafluoroethylene (PTFE) filter. The particles are then irradiated with light in the mid infrared range of 2,500 to 25,000nm which is then absorbed by the particles molecular bonds at characteristic frequencies (Takahama et al. 2019). The resulting spectra can then be used to characterize the organic and inorganic functional groups that contain the irradiated molecular bonds (Takahama et al. 2019). The majority of these techniques use optical, thermal optical, or acoustic methods to determine the BC fraction. Few techniques characterize the chemical signature; of these Raman Spectroscopy has emerged as a novel and viable method for on-line BC chemical identification.

3.1.3 Raman Spectroscopy

Raman spectroscopy (RS) is an optical technique that relies on the inelastic scattering of a monochromatic light source, typically in the visible range. RS is similar to infrared spectroscopy, in that each measures vibrational frequencies of a molecule; these frequencies can be used to identify compounds. RS has been successfully used to characterize biological material. Previous studies include the compilation of a micro-fungi spectral library used to identify unknown micro-fungal spores through direct comparison (Ghosal, Macher, and Ahmed 2012). RS has also been used to characterize pollen samples from many different plant species (Ghosal, Macher, and Ahmed 2012). In addition to biological compounds, RS has also been used in the characterization of aerosols such as BC. RS provides chemical characterization of particles with higher sensitivity than many techniques, but less than others such as mass spectroscopy. Its capability for chemical speciation of a larger range of materials than available with most techniques, makes it an ideal tool to characterize compounds made of several different molecules such atmospheric aerosols (Sze et al. 2001). Raman spectra associated with BC molecules normally exhibit peaks, known as D and G bands near 1320 and 1590 cm^{-1} as a result of vibrations within the graphitic lattice of the carbon molecule (Sadezky et al. 2005). The D bands occur due to the breathing mode, or expansion and contraction, of sp^2 hybridized carbon atoms within a ring (Ferrari 2007). The G bands are a result of the expansion of sp^2 hybridized atoms in chains and rings (Ferrari 2007). These peaks occur for almost all forms of BC and make it a distinguishable molecule when analyzing Raman spectra of aerosols.

The earliest studies of atmospheric BC using Raman spectroscopy date back to the late 1970’s (Rosen and Novakov 1977). In this project, BC particles were collected from diesel exhaust, automobile exhaust, and ambient air samples. The Raman spectra of these particles were compared to known Raman spectra of activated carbon and polycrystalline graphite. Rosen and Novakov found that the BC particles collected from their samples were physically similar to activated carbon and were the predominant species in vehicle exhaust and ambient samples (Rosen and Novakov 1977). These findings spurred further research into the Raman characterization of BC, and other atmospheric aerosol particles (Ault and Axson 2017). For example, Jawhari et. al collected several microscopic samples of commercially available BC analogs, characterized them using Raman Spectroscopy and, established correlations between the spectra and the molecular structure (Jawhari, Roid, and Casado 1995). Studies have also been conducted on the Raman characterization of other carbonaceous aerosols. In one such study, various carbonaceous particles were sampled onto quartz fiber filters (Sze et al. 2001). The Raman Spectra were then recorded directly from the filters and the relative Raman intensities of the carbonaceous aerosols were compared. These measurements, while unique, relied on batch collection of carbonaceous material. Furthermore, these studies were unable to produce quantitative measurements regarding the size and concentration of particles (A. Petzold et al. 2013). Recently, RS instruments have been built to collect aerosol particles and measure their Raman Spectra in real time (i.e., typically 10 to 50 minute delay) (Doughty and Hill 2017; Grafen et al. 2015, 2018). However, only Doughty and Hill study the Raman spectra of single particles. In both Grafen studies, the bulk carbonaceous material was imaged using RS. A single particle analysis of BC allows for the determination of aerosol mixing states and the effect on radiative forcing (Jacobson 2001; Sobanska et al. 2012). In the Doughty and Hill paper, an automated Aerosol Raman Spectrometer (ARS, generic name), known as the Resource Effective Bio-identification System (REBS), also more recently termed the Rapid Enumerative Bio-identification System (REBS), developed by Battelle (Columbus, OH) is operated semi-continuously to collect aerosol particles and analyze their Raman Spectra (Doughty and Hill 2017). Previous work has shown that a majority of Raman Spectra measured with the REBS in urban locations exhibit the D and G bands that are consistent with BC (Doughty and Hill 2017). However, because the Raman cross sections of BC are high compared with the great majority of other molecules, this information was limited and provided little to no information regarding the size and concentration of the BC particles. If a correlation between particle size, concentration, and Raman intensities can be established, RS will become significantly more useful as a method to characterize the and physical and chemical nature of BC and other atmospheric particles.

In this chapter, we explore the relationship between the size of BC particles and their measured Raman intensities. We wish to determine if there is a correlation between the two properties and if so, determine the minimum size of BC particles visible using RS. We recognize that this correlation likely depends upon the type and form of the BC, such as whether the soot is fresh and fractal, or processed through water and more dense. We also analyze the Raman spectra of ambient air measurements in an effort to determine the BC composition of particulate matter in the area of interest. We will rely on the REBS in order to obtain the Raman spectra of our samples. However, the sampling procedure will be modified with instruments that allow us to measure size and concentration of particles before they reach the ARS while also obtaining single particle deposition of aerosols.

3.2 <u>Methodology</u>

Multiple sources of BC are used in the experiment. Initially, Printex® (Orion), a powdery, ink-like BC analog was used as the BC source in this experiment. Printex® has been used in several previous biological studies into the health effects of black carbon (Heinrich et al. 1994; Gallagher et al. 2003) It has also been previously characterized using Raman Spectroscopy (Jawhari, Roid, and Casado 1995). However, since one of the primary sources of BC is burning of fossil fuels, and unprocessed, fresh soot is highly fractal with a low density, experimental burns of different materials were also used to generate BC particles. These materials included wax candles, gas burners, charcoal, and cellulose.

Wet and dry sampling of BC was conducted in this study. In the dry sampling, a BC source was put in a closed chamber. Clean air was supplied to either dilute the sample or provide oxygen for the flame. An outlet line sent the particles to the rest of the instruments. In wet sampling, BC aerosols were generated using a constant output atomizer. In this process, BC is suspended in water and placed in a sealed bottle. Pressurized air is then blown in, and droplets that contain the particles are sent out of the bottle, through a neutralizer, and into a heated pipe and dryer to remove any moisture before the resulting particles reach the other instruments.

Regardless of their sampling method, particles were size selected according to mobility diameter using the DMA (TSI 3080). Particles were size selected for mobility diameters between 100 and 500nm. The concentration of particles was monitored using the TSI 3787 Water CPC. These instruments have been characterized and used extensively in the study of a wide array of aerosols including BC (Novakov and Corrigan 1996; Slowik et al. 2007). Once the particles have been size selected and the concentrations have been determined, the particles are then sent to the ARS for the Raman spectra to be measured.

In the ARS, the particles are charged using a corona charger and drawn to a grounded, metallized tape. Once the sample has been deposited onto the tape, it is advanced to the confocal objective where they are imagined using a line scanning Raman spectrometer. In a line scanning spectrometer, instead of targeting a specific particle, a predefined sampling area is automatically focused and imaged. In the confocal objective a 50mW laser at a wavelength of 640 nm is focused into a single line on the sample tape with a width of 1 µm and a length of 40 µm (Doughty and Hill 2017). As the laser is focused on the sampling tape, a 128x1024 pixel charged coupling device (CCD) records the Raman scattering of the particles deposited on the tape (Doughty and Hill 2017). The 40 micron length of the laser corresponds to roughly 40 of the 128 pixels of the CCD. Each pixel targets an area of roughly 1µm x 1µm. Since the width of the laser is also 1 micron, this results in roughly 40 Raman spectra being taken in a single image. The tape is then advanced a predetermined distance, and the laser line refocuses and images over the next sampling area. Since particle deposition is random, particles can fall in the center of a pixel, or on the boundaries of one or more pixels, depending on the particle size. The appearance of similar peaks in adjacent laser lines within the same image is usually indicative of a particle that has fallen within the boundary of two vertical pixels. The appearance of similar peaks at the same laser line in adjacent images usually indicates particles have deposited within the boundary of two or more horizontal pixels. In either case, the measured Raman intensities are summed in order to determine the Raman intensity of the entire particle. However this summation of intensities may not be as accurate as the value that would have been obtained from the ARS had the particle fallen within one pixel. The laser refocuses after each scan which can cause slight changes in laser intensity and the measured Raman spectra, even when the same particle is being imaged. Thus, even for particles of the same size, slight variations in the measured Raman intensities is expected.

All of the instruments within this system are limited in terms of the concentration of particles they can handle. Thus, a dilution flow of clean air is added to the system in order to limit the concentration of particles entering the instruments. The flow configuration of both the dry and wet sampling are shown in figure 3.2.1 and 3.2.2.

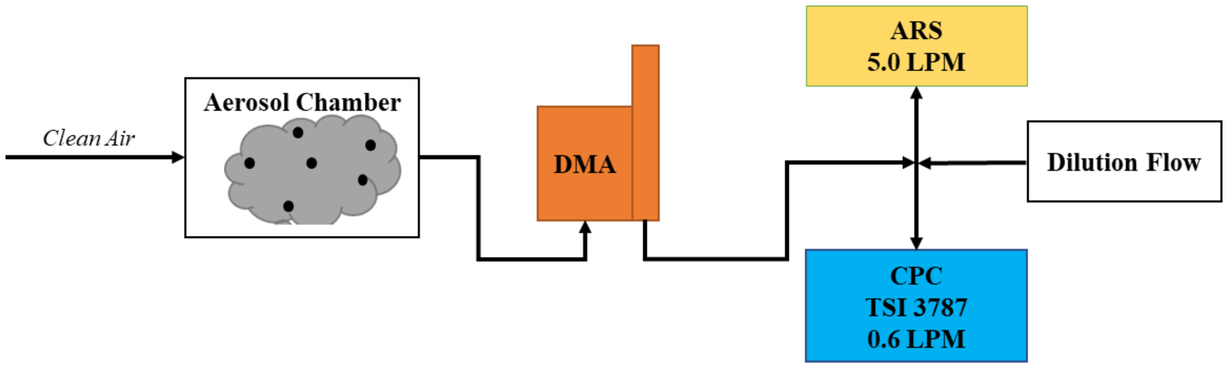

Figure 3.2.1 Flow Configuration of Dry BC Sampling

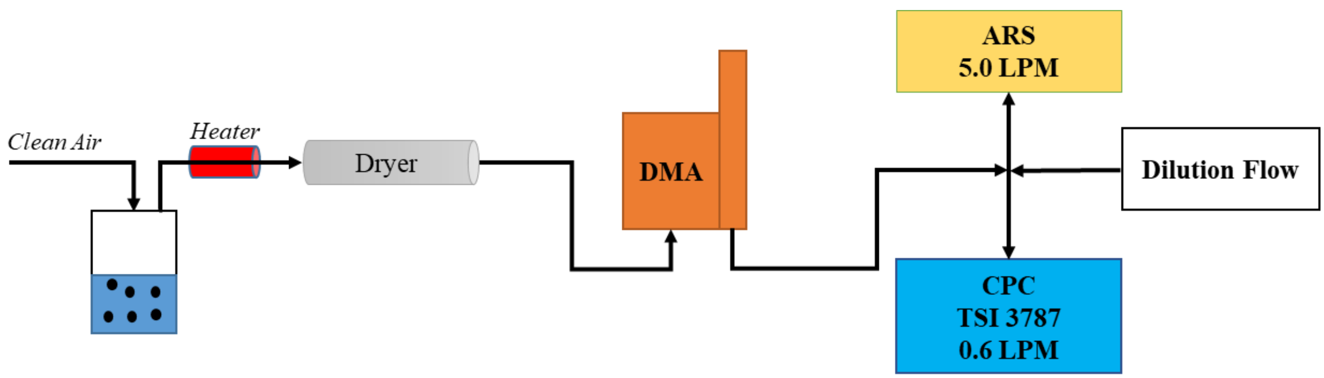

Figure 3.2.2 Flow Configuration of Wet BC Sampling

3.3 Results & Discussion

3.3.1 Control Particles

Before sampling BC particles we must first establish that the ARS is able to image submicron particles of any composition. This was illustrated using polystyrene latex (PSL) spheres. PSL has been used extensively in aerosol research and has a known Raman spectra peak location. The PSL particles used in this experiment were Nanosphere™ Size Standards from Thermo- Scientific. These spherical particles are separated according to their mean diameter and suspended in water. To aerosolize them, we added between 5-20 drops of the PSL solution to a container of nano-pure water and placed it in our constant output atomizer apparatus. The mean particle sizes sampled were 150, 300, and 500 nanometers.

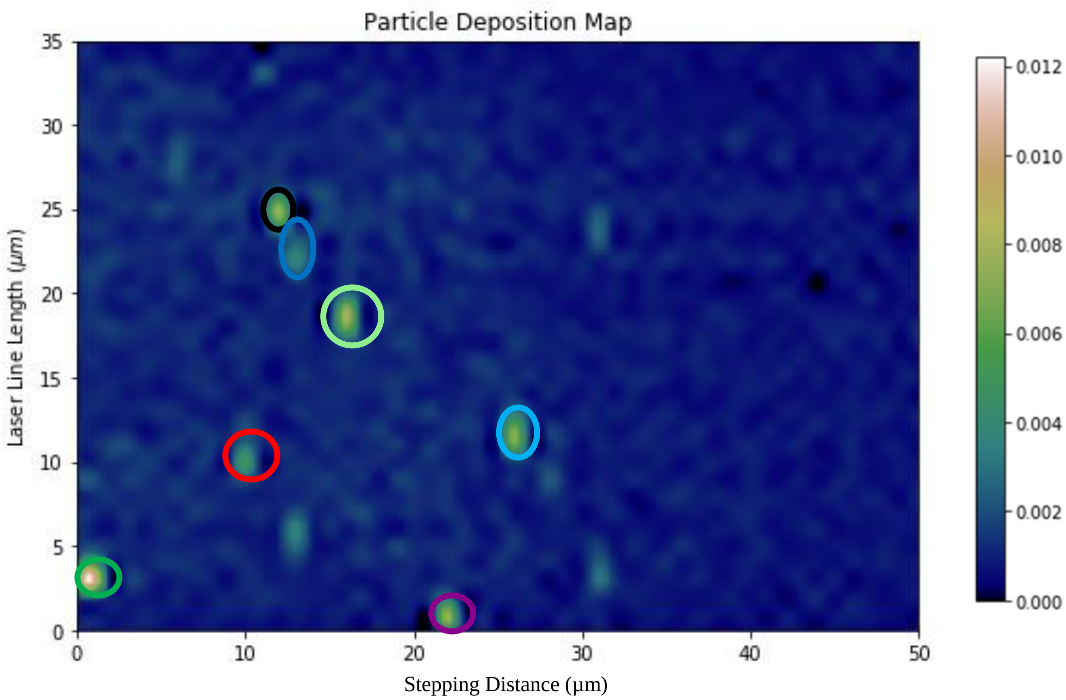

Figure 3.3.1 Raman Intensity Image of 300nm PSL Spheres with 7 particles selected

Figure 3.3.1 shows the deposition of 300nm PSL particles at a (in air concentration of about 100 particles per cm^3) along the ARS sampling tape. Particles were sampled onto the tape for 30 minutes and then imaged for one hour. The y-axis is the vertical height of the laser while the x-axis is the horizontal stepping distance along the tape. For each horizontal step, a Raman spectra image similar to Figure 3.3.2 is obtained. In this image, the horizontal line represents the Raman spectra of the single micron of the laser line length from the particle deposition map. The spectra are offset to prevent overlap and ensure the spectra are understandable. The horizontal axis or, Raman shift, represents the frequency shift of the particle's electrons as it is irradiated by the laser within the ARS. The Raman shift of a particle is dependent upon its molecular structure. If a particle is present in the imaging area, a peak should appear at an appropriate Raman shift. For phenyl hydrocarbon compounds, such as PSL, a sharp peak can be seen at about 1000 cm^{-1}.

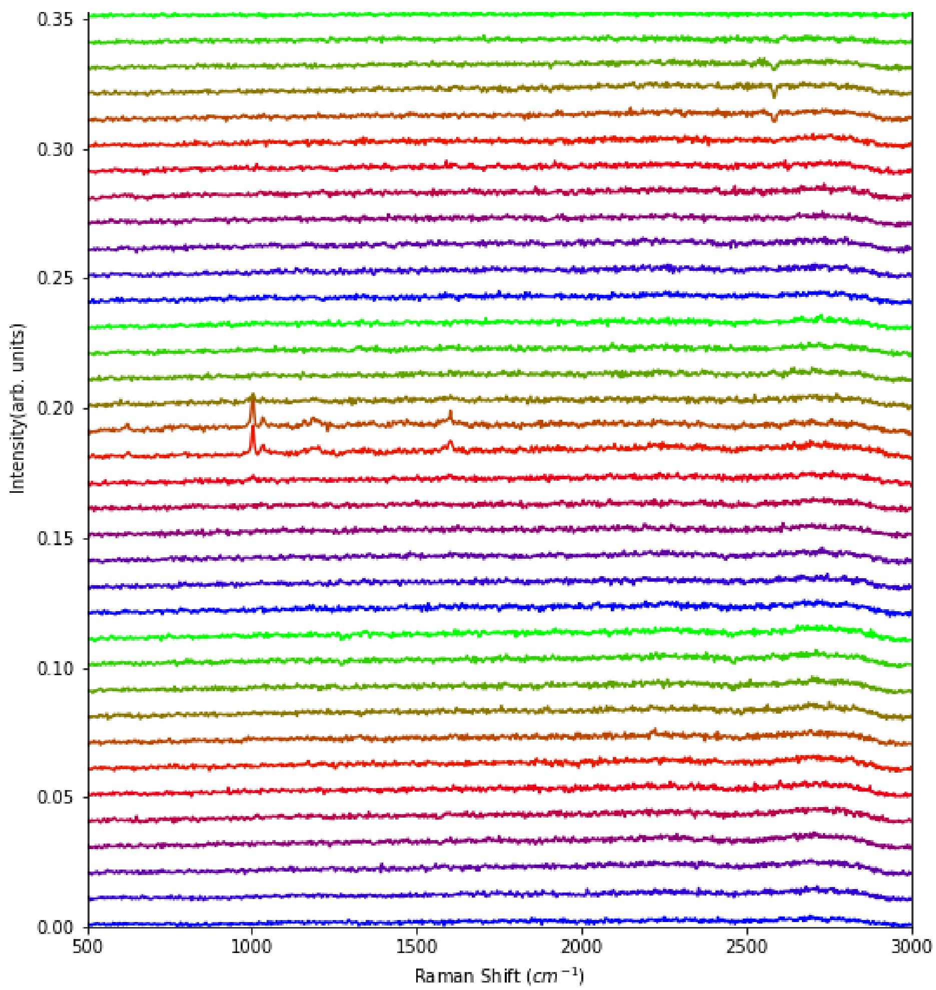

Figure 3.3.2 Single Raman spectra taken during sampling of 300nm PSL particles

The PSL particles in this study are spherical, of known diameter, and have also been size selected according to their mobility diameter using the DMA. Thus, the particles are assumed to be identical and should have the same Raman intensities. In order to verify this all of the Raman Spectra consistent with PSL are plotted together and their Raman intensities are compared in Figure 3.3.3.

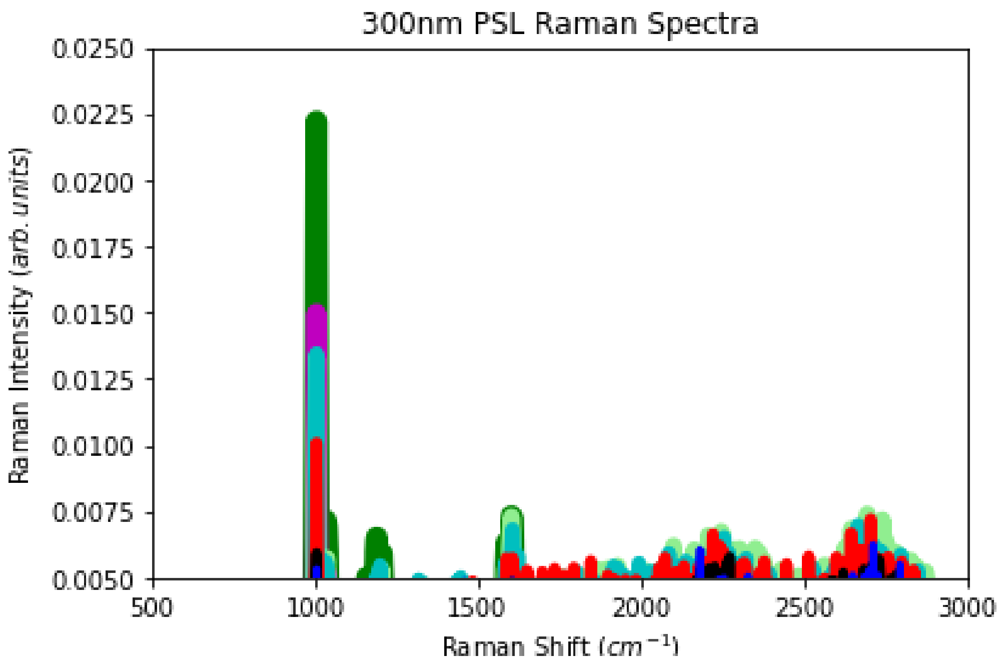

Figure 3.3.3 Raman Spectra Comparison of 300nm PSL Nanospheres (images from 7 particles selected in figure 3.3.2)

In this figure, we have all of the readable Raman spectra for the 300nm PSL sample plotted against one another. We see there are variations in the Raman intensity at the characteristic PSL peak at 1000 cm^{-1}. However, these variations change by a factor of 5 from 0.005 to 0.025. These relatively small deviations suggest that there is considerable agreement amongst the Raman intensities of PSL and that we are likely imaging submicron particles.

3.3.2 Dry BC Sampling

Using the dry sampling process depicted in Figure 3.2.1, we initially examined the Raman spectra of Printex® particles and ambient air. Particles were again mobility size selected for 300nm, collected for 30 minutes, and imaged for one hour. Figure 3.3.4 shows the deposition along the ARS sampling tape for the Printex®. In both cases, adequate deposition is achieved and Raman spectra that exhibit the D and G bands associated with BC are obtained at near 1300 and 1600cm^{-1} respectively.

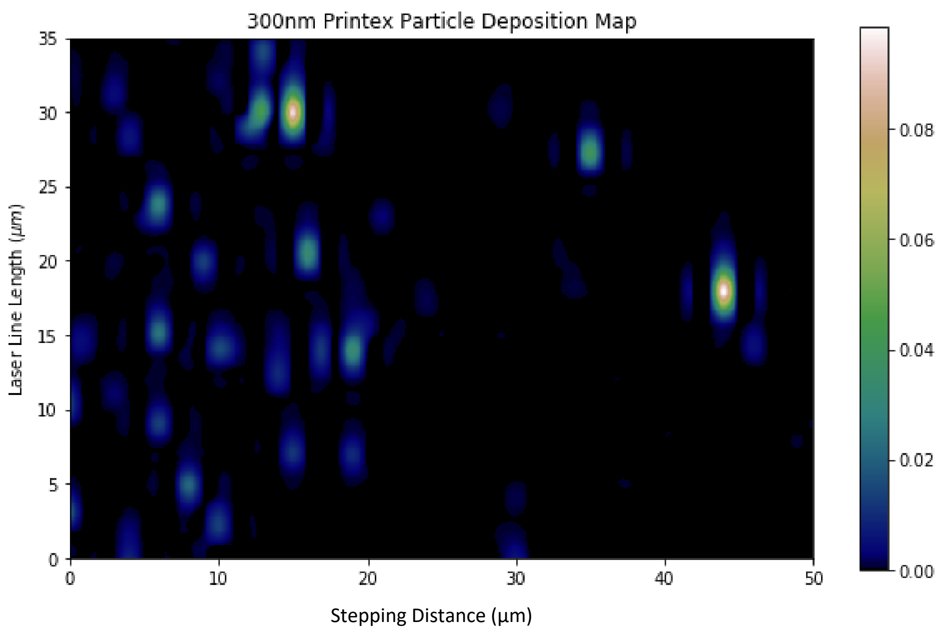

Figure 3.3.4 Raman Intensity Image of 300nm Printex® Particles

In Figure 3.3.5, we see quite a few D and G peaks meaning more than one particle is within the area of this scan. We also see that unlike the PSL, the peaks span across multiple laser lines. If peaks appear on the same laser line, and in consecutive images, this indicates that a particle may have fallen on the boundary between the steps of the laser. In cases like these, such as in Figure

3.3.5 the intensities across all images are summed together to give a more accurate representation of the particles intensity.

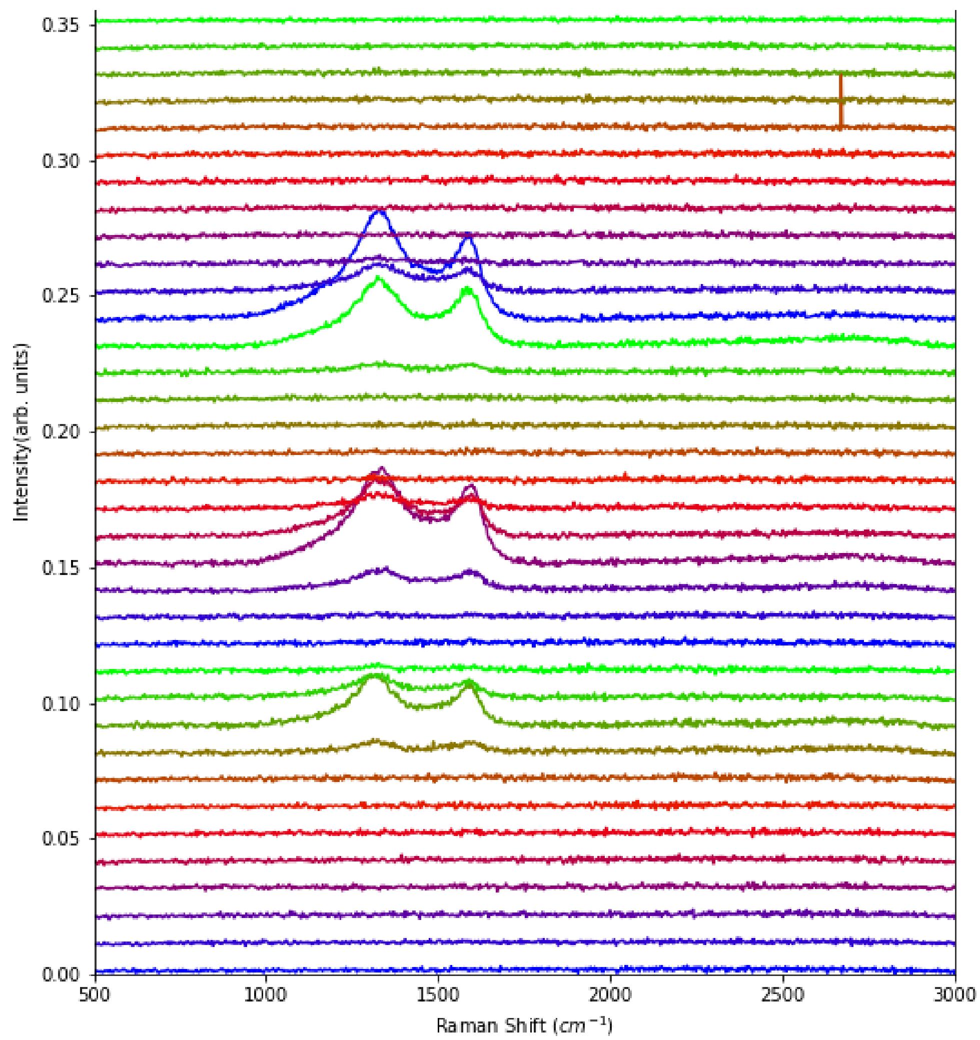

Figure 3.3.5 Single Raman spectra taken during sampling of 300nm PSL particles

Unlike the near uniformity of the PSL spheres, the Raman spectra of the Printex® particles exhibit larger variations in Raman intensity. Figure 3.3.6 shows that for mobility size selected particles, Raman intensities vary by more than a factor of 10. Variations in the Raman intensities of the air sample (See Appendix) are expected due to the unknown composition of BC in ambient air. However for Printex®, differences of this magnitude, for particles that have been mobility size selected for 300nm, were surprising. This indicates that agglomeration of particles has occurred. This is confirmed when we use a scanning electron microscope (SEM) to view the ARS sampling tape with Printex® deposited on it.

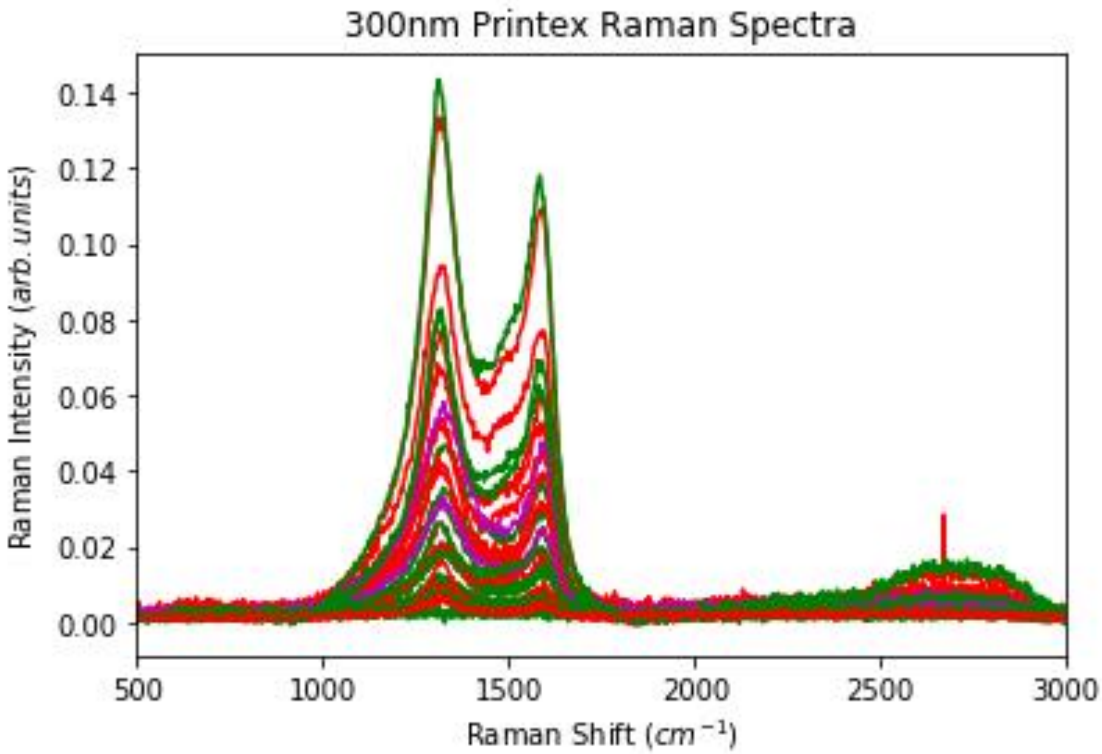

Figure 3.3.6 Raman Spectra Comparison of 300nm Printex®

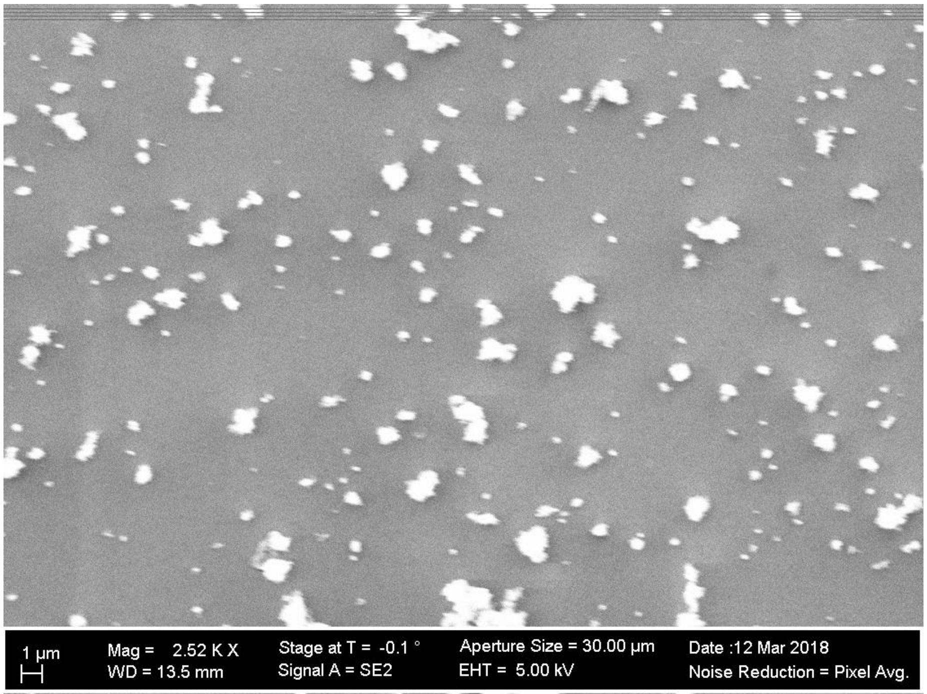

Figure 3.3.7 SEM Photograph of 300nm Printex®

Figure 3.3.7 depicts a Sample of 300nm Printex® that had been size selected for 300 nm particles. Here we see that particle size is not uniform. There are several Printex® agglomerates present, with some even larger than 1 micron. In an effort to mitigate this agglomeration issue within our system, we decided to sample black carbon from freshly burned material and compare the Raman spectra of these particles to those of Printex®. We chose to burn coal, wax candles, gas burners, and cellulose. Of those burns, only the cellulose and wax candle produced detectable particles. The burn particles were size selected for 300nm and 500nm respectively. In this case particles were sampled for 15 minutes and imaged for another 15 minutes. In each case, the Raman spectra showed less variation than that of the Printex®. However, only 2 particles were deposited in each of these samples, making it difficult to compare them to Printex® and resolve the agglomeration issue.

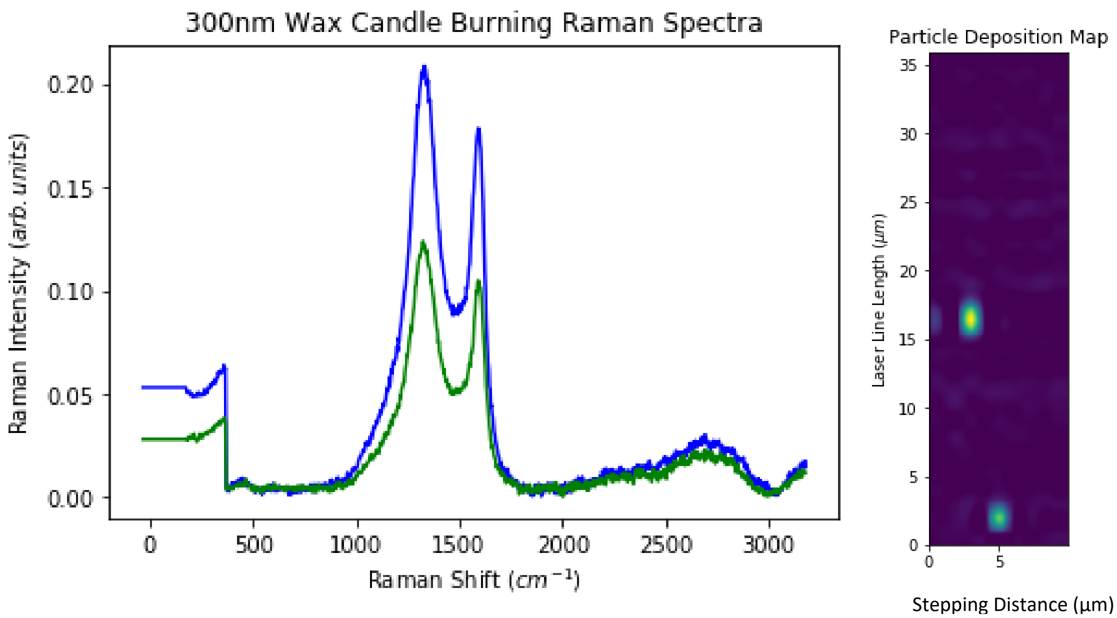

Figure 3.3.9 Raman Intensity Image and selected Raman Spectra of 300nm Size selected Wax Candle Burn Particles

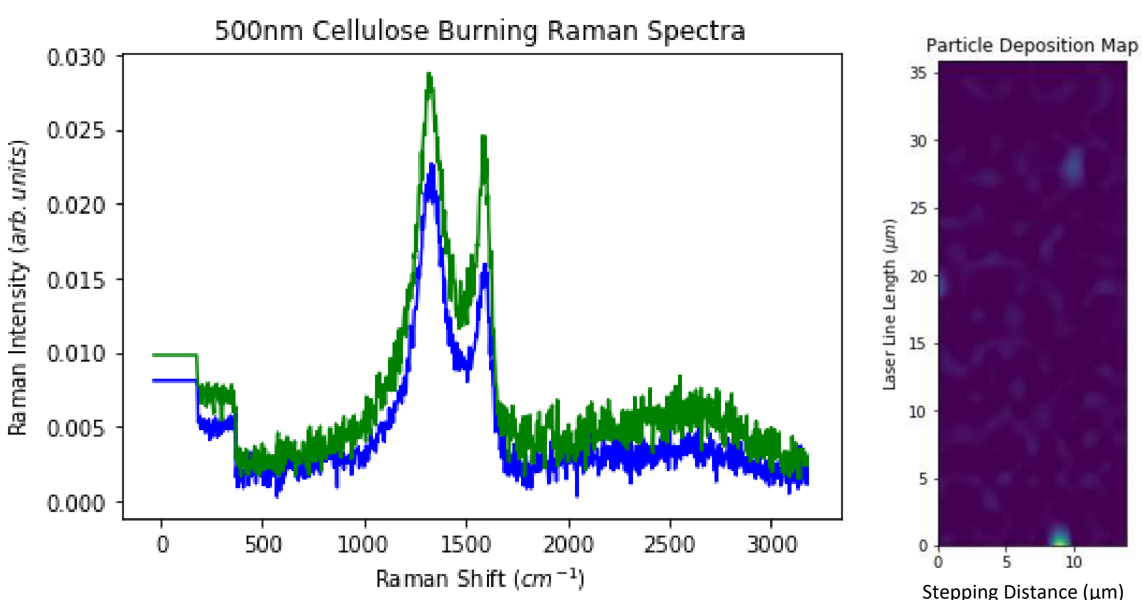

Figure 3.3.10 Raman Intensity Image and selected Raman Spectra of 500nm Size selected Cellulose Burn

3.3.3 BC Atomization

Printex® appeared to be having issues with agglomeration using our dry sampling technique. Thus, we decided to use the same wet atomization technique used for PSL spheres. Forty milligrams of Printex® was mixed with 250 ml of nano-pure water to create a stock solution. Portions of it were then severely diluted in order to produce desirable number concentrations of Printex® particles and analyze the Raman spectra of 100, 200, and 300 nm mobility size selected particles.

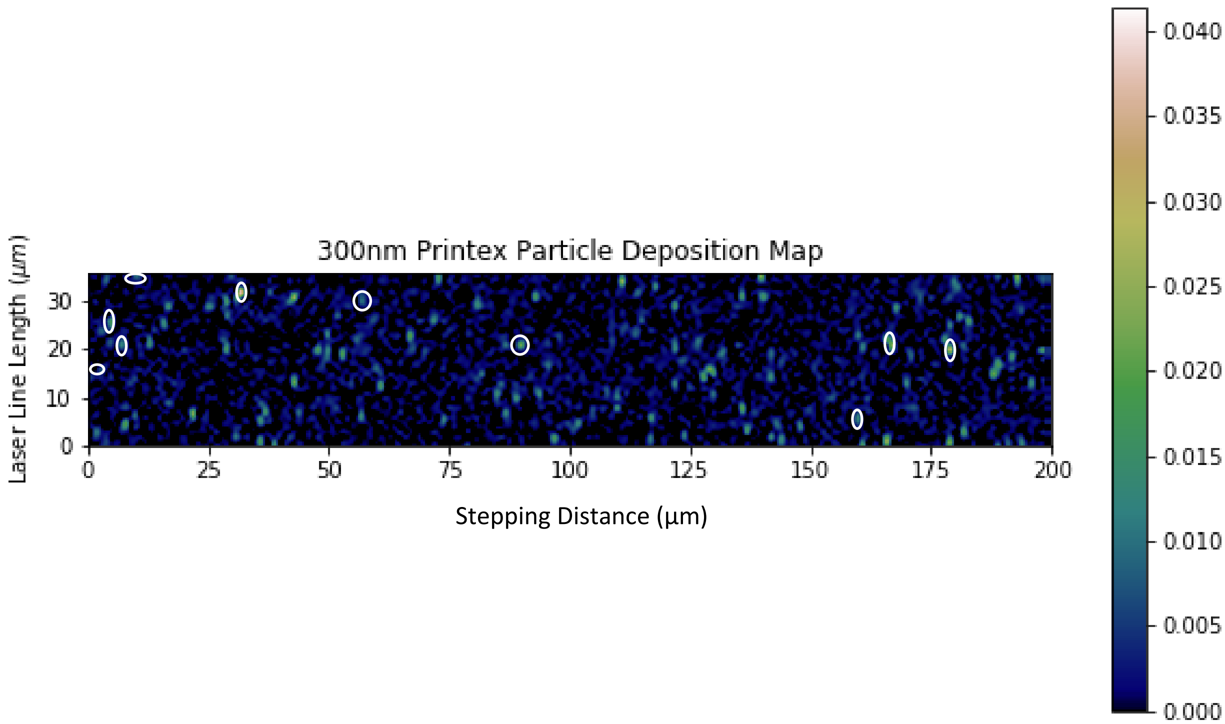

Figure 3.3.11 Raman Intensity Image of 300nm Atomized Printex® *(random particles selected in white)*

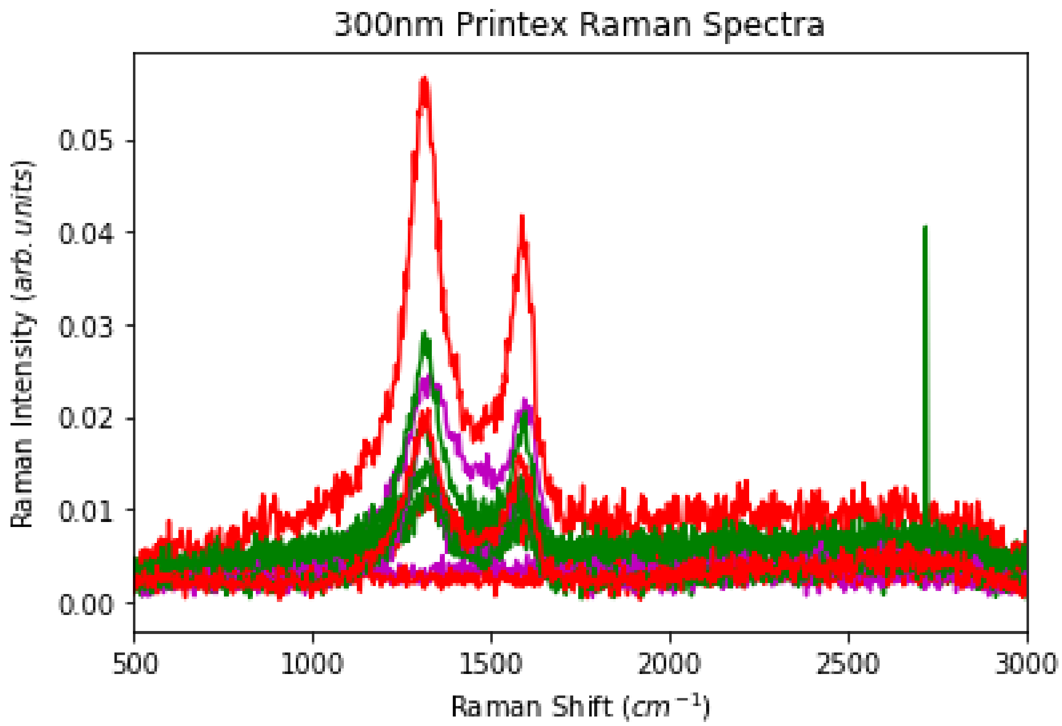

Figure 3.3.12 Selected Raman Spectra of 300nm Atomized Printex® Particles

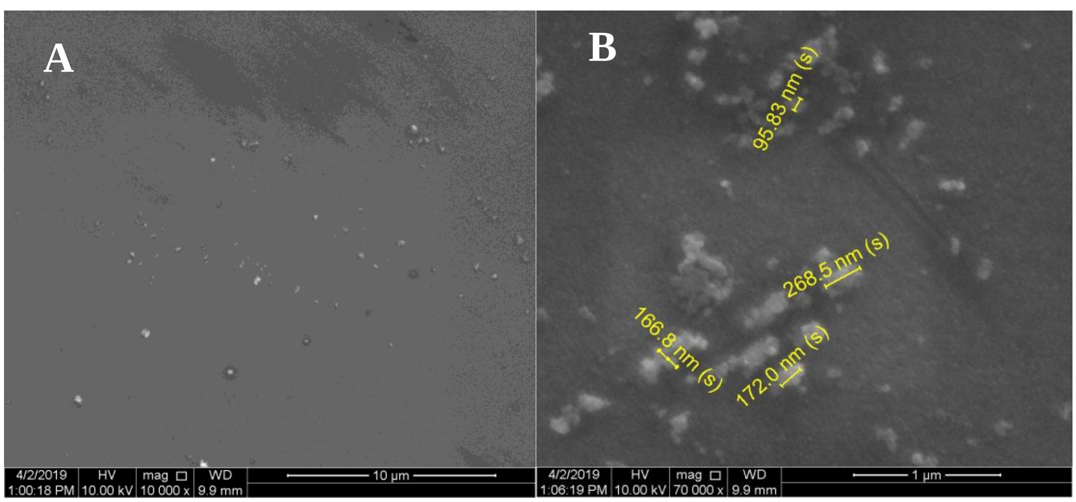

Figure 3.3.13 SEM Photograph of 300nm Atomized Printex® Particles at scales of 10µm (A) and 1µm (B)

Figure 3.3.11 shows the particle deposition for 300nm mobility size selected particles of Atomized Printex®. The map is noticeably longer because the imaging time was increased from one to three hours to analyze a larger area of the tape. Initial image times of 30 minutes did not capture any Raman Spectra of the Printex® particles. Figure 3.3.12 presents a few of the spectra gathered from the images. We see that not only has the magnitude of the peak height decreased but the variation has as well. However, these are only a few of the spectra within the large sample, a rigorous comparison of all spectra is need to determine the similarity between the measured intensities.

The SEM photographs in Figure 3.3.13 show that the particles are much smaller than those obtained from the dry sampling. While they are not uniform at 300nm, there appear to be no super-micron particles. It is also essential to note that these particles have been size selected according to their electric mobility. SEM images are taken by placing a specimen between two cathode ray tubes (Leamy 1982). As one cathode bombards the sample with a focused beam of electrons, the other detect the disturbance and builds and image of the sample (Leamy 1982). This leads to SEM images being heavily influenced by the physical characteristics of the sample. This is largely different from the DMA which size selects according to electrical mobility and due to charging that occurs within the instrument, a small number of multiply charged particles is produced and the resulting aerosol is not monodisperse (Tavakoli and Olfert 2014). If the particles were spherical, as is the case with PSL, then the two diameters would be equivalent. BC however, is not spherical and characterized by its graphitic structure. Thus the mobility diameter measured by the DMA and the physical diameter given by the SEM would not be expected to agree.

3.4 Conclusion

In this chapter we set out to establish a quantitative relationship between the measured Raman intensities of submicron BC particles and particle size. While we were unable to definitively state the relationship between the size and Raman intensity of BC particles, we are able to detect Raman spectra that appear to be consist with BC between 100-500nm mobility diameters. We also established that wet sampling of BC appears to yield more consistent BC size. Given the non-spherical nature of BC, future studies should size select BC particles that use sampling methods or instrumentation that account for their physical characteristics. One such instrument is the Aerodynamic Aerosol Classifier (AAC). This instrument size selects particles according to their relaxation time which can then be used to find the aerodynamic diameter, which does not assume particles are spherical (Tavakoli and Olfert 2014). This will lead to the production of a truly monodisperse aerosol. If the BC particles are truly uniform in size, we could definitively state that particles are indeed BC using RS and quantify the relationship between size and Raman intensity.

Chapter 4: Conclusions and Future Work

4.1 Conclusions

In this thesis, we studied various methods for measuring the physical properties and chemical composition of atmospheric aerosols. Increased emissions of particulate matter pose a significant threat to global human and environmental health. Their plethora of emission sources and ability travel extensively makes them difficult to measure and mitigate. This is why we rely on regulatory agencies such as the EPA and their regional counterparts to monitor air quality. We used our instruments to gather local particulate matter concentration data and compared it to the regional values reported by our state environmental agency, the MDE. We found that while the MDE CPC's undercount particles, there is no significant variation in the particle number concentration between the two locations. This indicates that the MDE is well situated to determine regional concentrations within at least a 5-mile radius. We also found that there is no correlation between the mass concentration of $PM_{2.5}$ reported by the MDE, and the simultaneous number concentration obtained from the CPC's. This is as expected since the particle number distribution is skewed towards the smaller particle sizes, sizes which are not even considered in mass distribution. These smaller particles are the most detrimental to human health and the environment. Continued reliance on mass concentration to report on the amount fine particulate matter will result in continued underestimations. This study also briefly observed the effect of particle size on concentration in the form of a nucleation event. Observing physical atmospheric interactions, such as nucleation, will allow for a better understanding of how aerosols behave and could lead to solutions as to how we can prevent their harmful effects.

The chemical composition of aerosols is also essential to monitoring atmospheric particulate matter levels and their potentially hazardous effects. In this thesis, we examined BC in particular. BC has no lack of emission sources and its status as a carcinogenic and radiative forcing molecule make it an aerosol that must be physically and chemically characterized extensively. We presented a method to find a quantitative correlation between the size of a BC particle and its measured Raman intensity. The semi-continuous nature of the ARS provides chemical information about the compound from the Raman Spectra in real time (delay of 10-50 minutes) as opposed to other currently used chemical characterization techniques.

While we were unable to identify a direct correlation, by size selecting BC particles, and imaging them with the ARS we were able to establish a minimum threshold mobility diameter of 100nm for the detection of BC particles with RS.

4.2 Recommendations for Future Work

The work presented in this thesis has several areas that could be expanded upon. To begin, the regional particle concentration reported by the MDE should be compared to local concentrations further and further away from the monitoring site. This will allow for a boundary to be established for the station. Outside of its boundary, the air quality data reported by a monitoring station would not be accurate. This would create regions for air quality monitoring stations that provide its inhabitants with much more accurate information as opposed to relying on one station to report data for each county. Future comparisons of local and regional data should also obtain particle size distribution data in order to ensure a robust comparison of particle size. The current results from the comparison between Raman intensity and BC particle size look promising. However, a monodisperse aerosol would likely make it easier to identify the correlation between the two, if there is one. Studies show that the AAC currently has the capability to size select particles and release a monodisperse aerosols thanks to its measurement principles that do not rely on the assumption of spherical particles (Tavakoli and Olfert 2014). A change in the source of BC used in this experiment might also yield new findings. The burns conducted in this thesis did not produce many particles that were visible using RS. Many studies have used RS to characterize the emissions of vehicle exhaust lines (Malmborg et al. 2019; Ge, Ye, and He 2019). An exhaust line from a vehicle or its engine could be run into our system to get a constant source of dried BC particles.

Appendix A: Additional Figures from Field Measurements

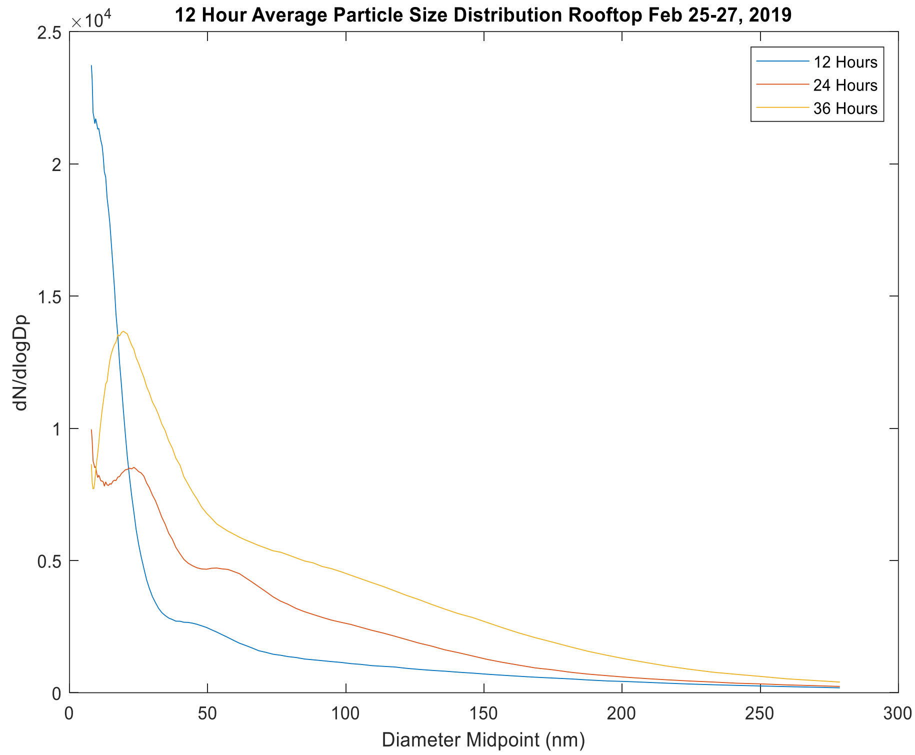

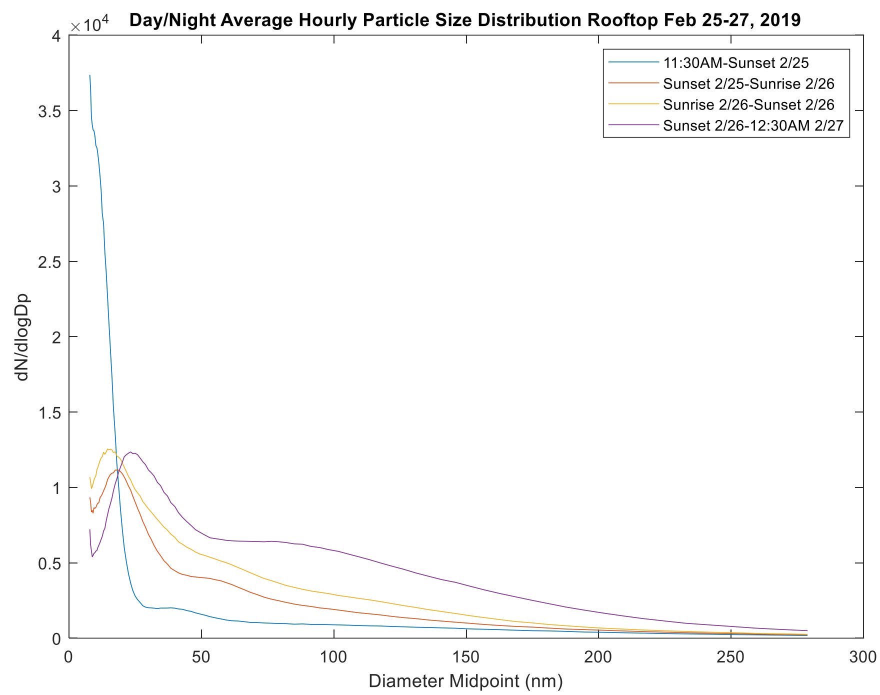

Figure A.1. Feb 25th -Feb 27th Particle Size Distribution at College Park Lab (12 Hour Avg.) Top, (Day/Night Avg.) Bottom

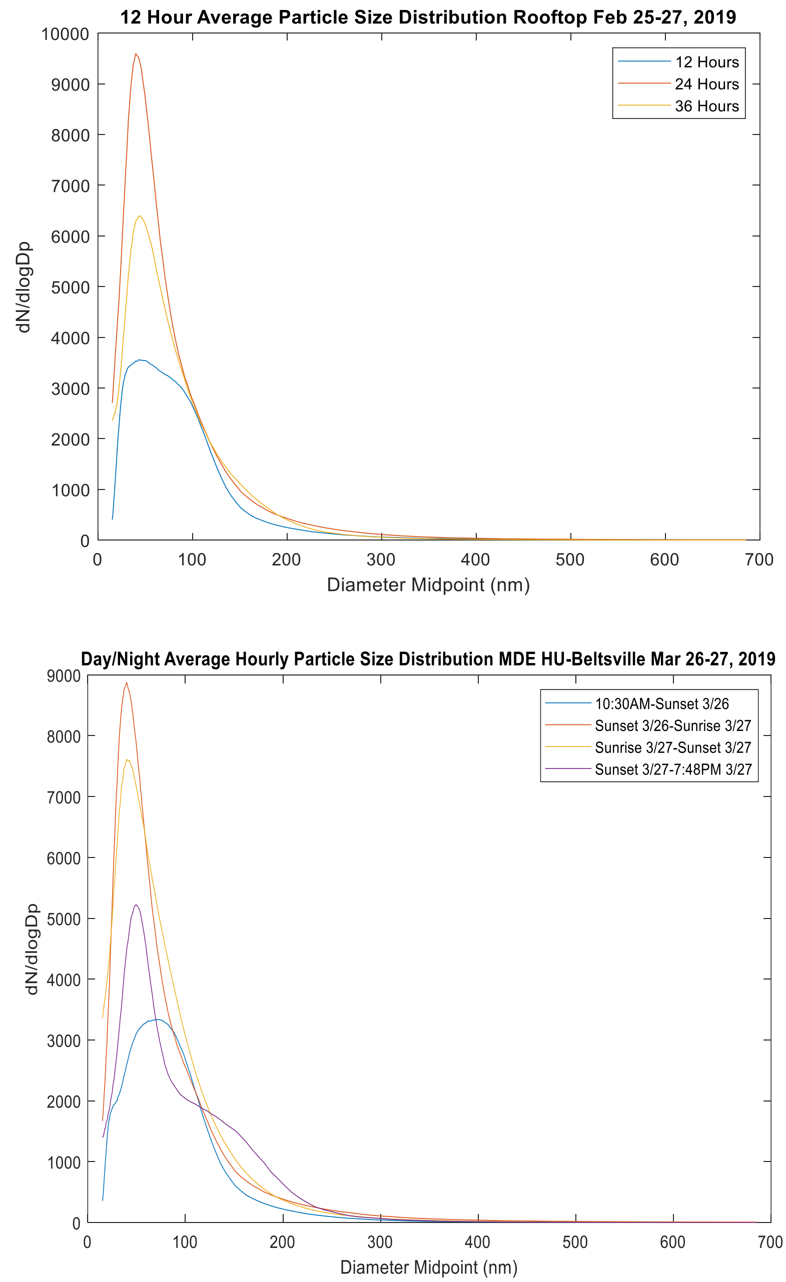

Figure A.2. Mar 26th -Feb 27th Particle Size Distribution at College Park Lab (12 Hour Avg.) Top, (Day/Night Avg.) Bottom

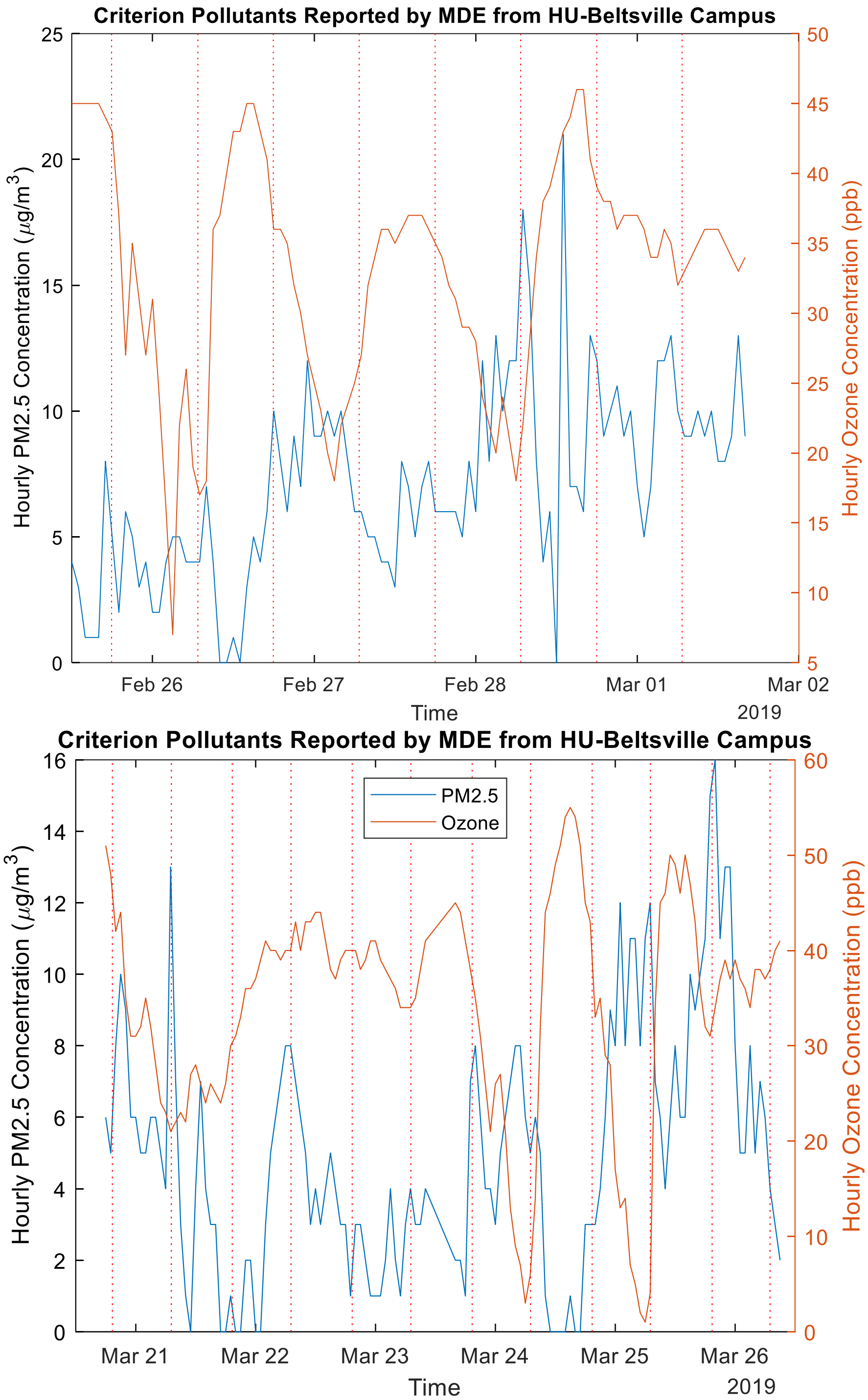

Figure A.3 Ozone and $PM_{2.5}$ Pollutant Concentration Reported During Sampling Periods

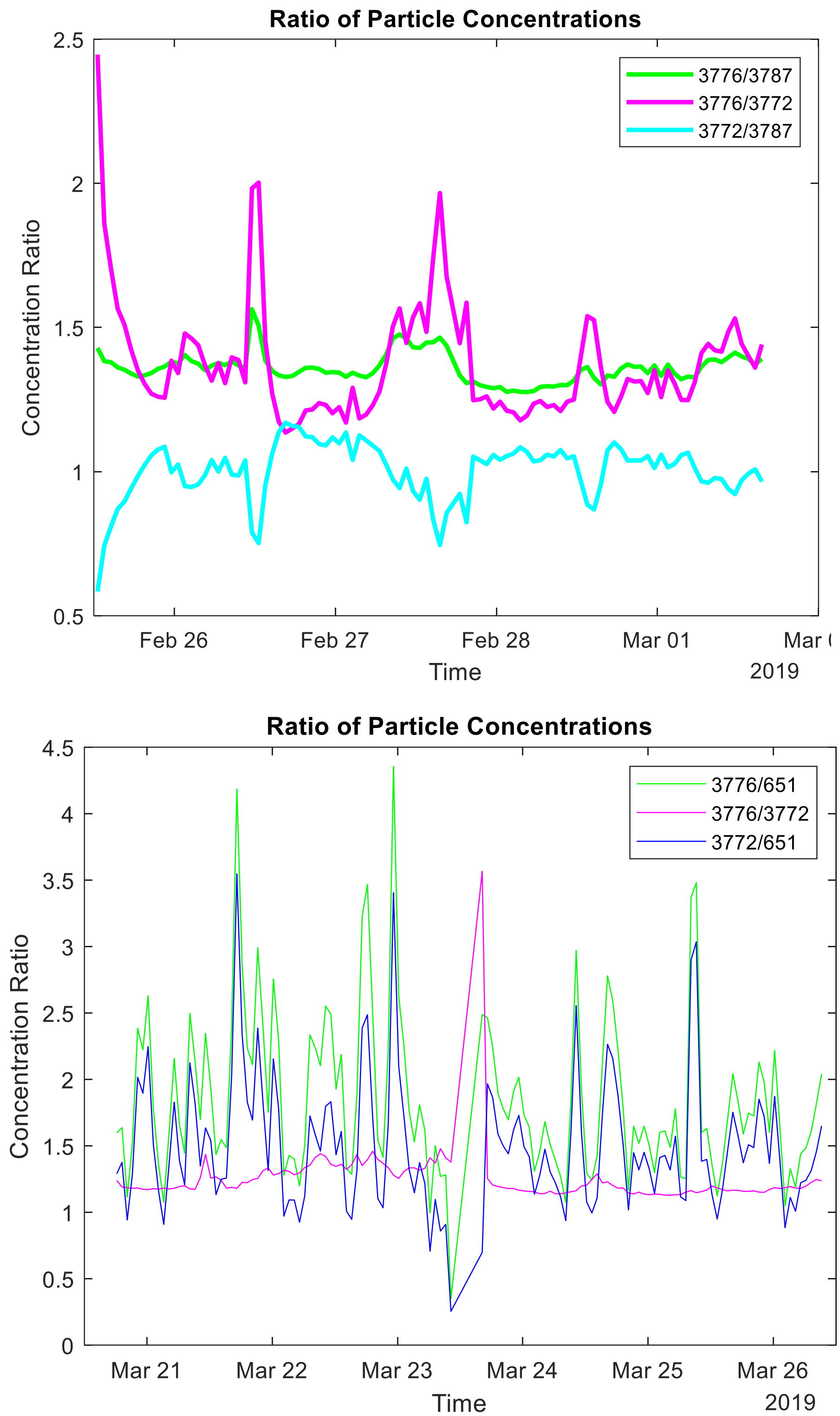

Figure A.4 Ratio of Number Concentration recorded between CPC's During Sampling Periods

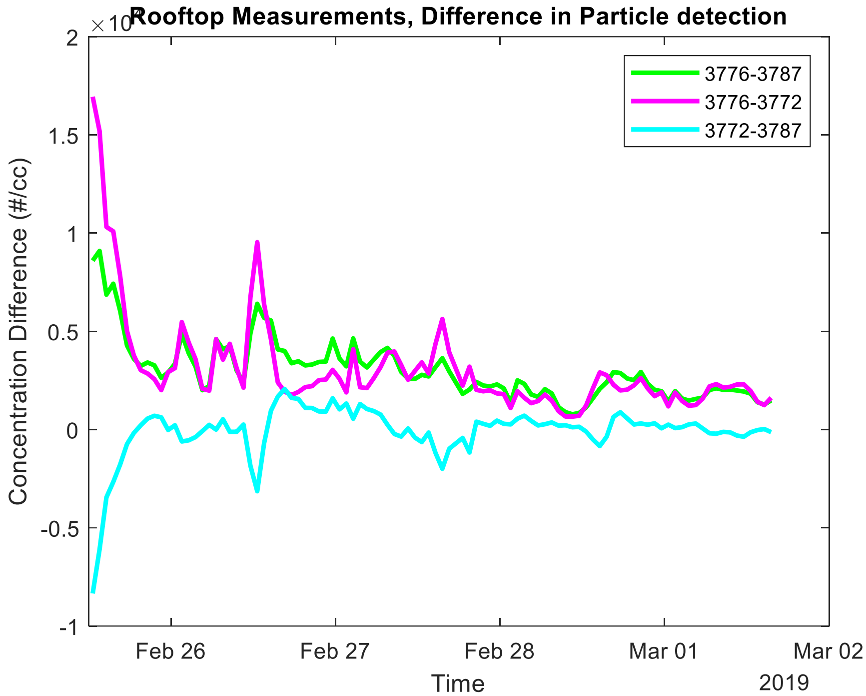

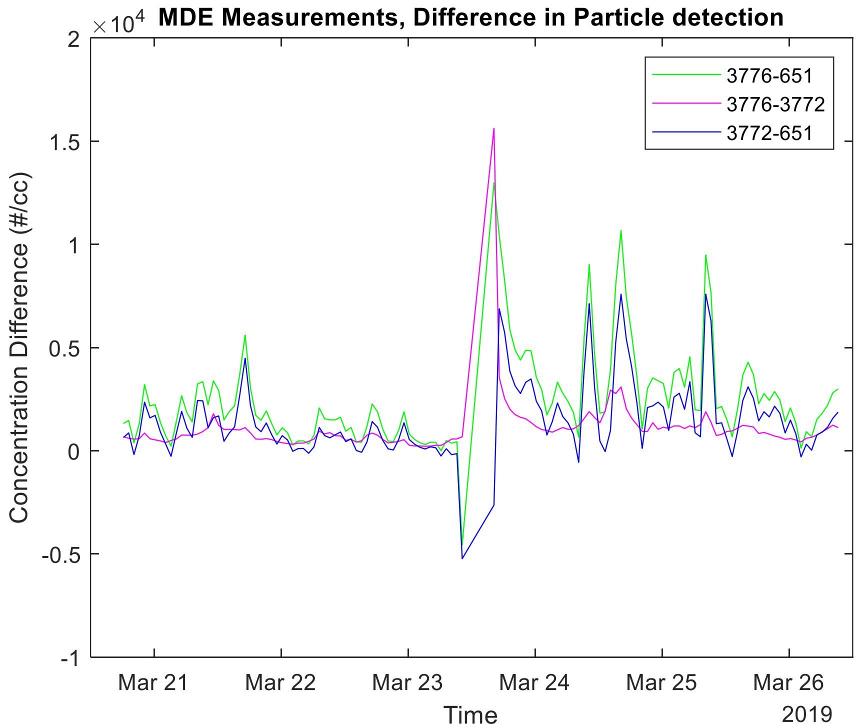

Figure A.5. Difference in Number Concentration recorded between CPC's During Sampling Periods

Appendix B: Additional Raman Spectra Images

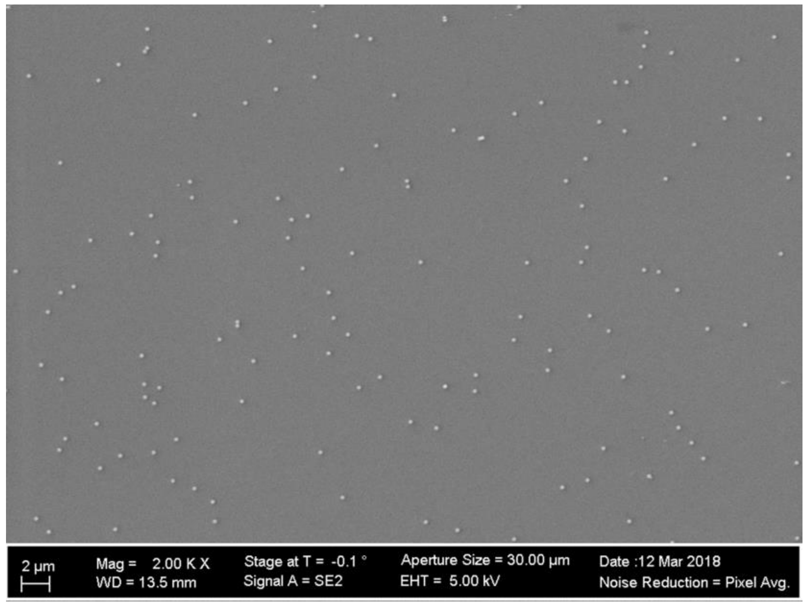

Figure B.1. SEM Image of 300nm Mobility Size Selected PSL

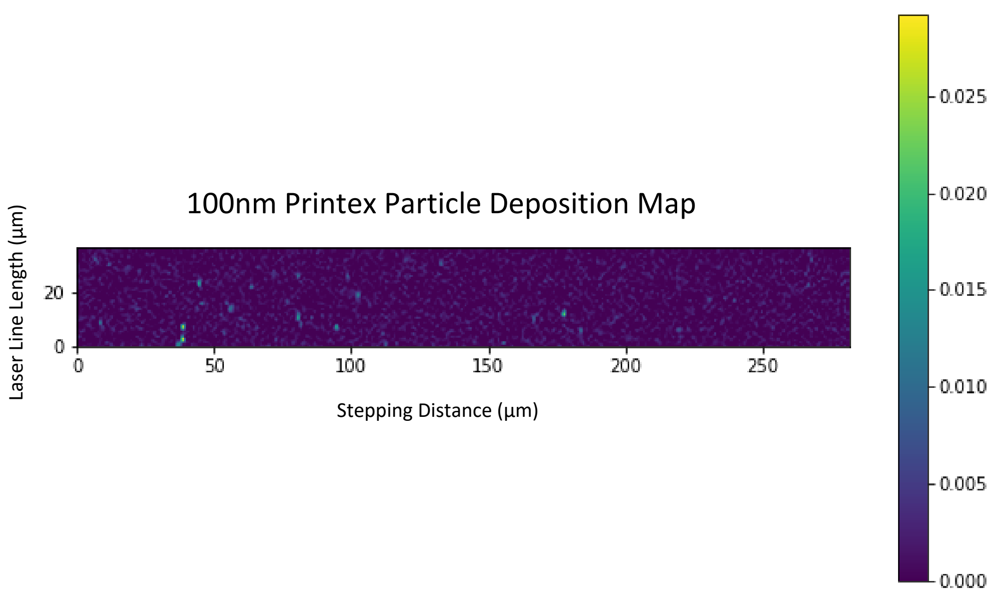

Figure B.2. Raman Intensity Image of 100nm (Atomized) Printex® Particles

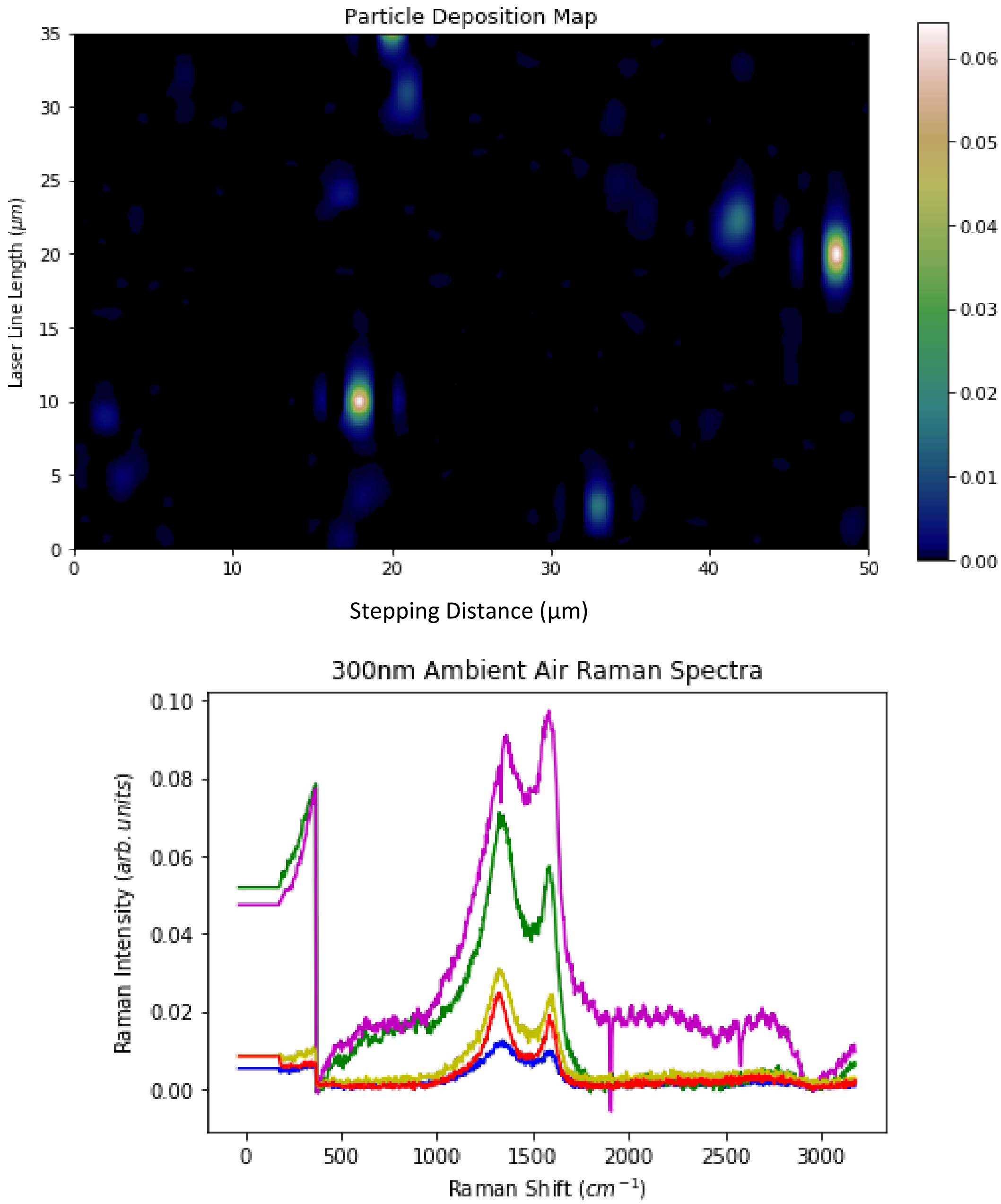

Figure B.3. Raman Intensity Image and Selected Raman Spectra of 300nm Ambient Air Particles

Bibliography

“Ambient Air Monitoring Network.” n.d. Accessed April 12, 2019. https://mde.maryland.gov/programs/Air/AirQualityMonitoring/Pages/Network.aspx.

Andreae, M O, and A Gelencser. 2006. “Black Carbon or Brown Carbon? The Nature of Light-Absorbing Carbonaceous Aerosols.” *Atmos. Chem. Phys.*, 18. https://doi.org/10.5194/acpd-6-3419-2006.

Ault, Andrew P., and Jessica L. Axson. 2017. “Atmospheric Aerosol Chemistry: Spectroscopic and Microscopic Advances.” *Analytical Chemistry* 89 (1): 430–52. https://doi.org/10.1021/acs.analchem.6b04670.

Carlton, A G, C Wiedinmyer, and J H Kroll. 2009. “A Review of Secondary Organic Aerosol (SOA) Formation from Isoprene.” *Atmos. Chem. Phys.*, 19. https://doi.org/10.5194/acp-9-4987-2009.

Charlson, Robert J., and Tom M. L. Wigley. 1994. “Sulfate Aerosol and Climatic Change.” *Scientific American* 270 (2): 48–57. https://doi.org/10.1038/scientificamerican0294-48.

“China: Air Quality Standards | Transport Policy.” 2018. 2018. https://www.transportpolicy.net/standard/china-air-quality-standards/.

Chylek, Petr, and J. Wong. 1995. “Effect of Absorbing Aerosols on Global Radiation Budget.” *Geophysical Research Letters* 22 (8): 929–31. https://doi.org/10.1029/95GL00800.

David D. Parrish, Jin Xu, Bart Croes, and Min Shao. 2016. “Air Quality Improvement in Los Angeles—Perspectives for Developing Cities.” *Frontiers of Environmental Science & Engineering* 10 (5): 11. https://doi.org/10.1007/s11783-016-0859-5.

Doughty, David C., and Steven C. Hill. 2017. “Automated Aerosol Raman Spectrometer for Semi-Continuous Sampling of Atmospheric Aerosol.” *Journal of Quantitative Spectroscopy and Radiative Transfer*, Advances in Atmospheric Light Scattering: Theory and Remote Sensing Techniques, 188 (February): 103–17. https://doi.org/10.1016/j.jqsrt.2016.06.042.

“Emission Standards: Europe: Cars and Light Trucks.” n.d. Accessed April 11, 2019. https://www.dieselnet.com/standards/eu/ld.php.

Esposito, Katherine, Giuseppe Bellastella, Maria Ida Maiorino, and Dario Giugliano. 2018. “Particulate Matter Air Pollution: Individual Choices for Improving Cardiometabolic Well-Being.” *Endocrine* 59 (3): 495–98. https://doi.org/10.1007/s12020-017-1326-1.

Ferrari, Andrea C. 2007. “Raman Spectroscopy of Graphene and Graphite: Disorder, Electron–Phonon Coupling, Doping and Nonadiabatic Effects.” *Solid State Communications* 143 (1–2): 47–57. https://doi.org/10.1016/j.ssc.2007.03.052.

Flanner, Mark G., Charles S. Zender, James T. Randerson, and Philip J. Rasch. 2007. “Present-Day Climate Forcing and Response from Black Carbon in Snow.” *Journal of Geophysical Research: Atmospheres* 112 (D11). https://doi.org/10.1029/2006JD008003.

Gallagher, J, R Sams, J Inmon, R Gelein, A Elder, G Oberdörster, and A.K Prahalad. 2003. "Formation of 8-Oxo-7,8-Dihydro-2′-Deoxyguanosine in Rat Lung DNA Following Subchronic Inhalation of Carbon Black." *Toxicology and Applied Pharmacology* 190 (3): 224–31. https://doi.org/10.1016/S0041-008X(03)00187-X.

Gershenzon, Jonathan, and Natalia Dudareva. 2007. "The Function of Terpene Natural Products in the Natural World." *Nature Chemical Biology* 3 (7): 408–14. https://doi.org/10.1038/nchembio.2007.5.

Ghosal, Sutapa, Janet M. Macher, and Kadra Ahmed. 2012. "Raman Microspectroscopy-Based Identification of Individual Fungal Spores as Potential Indicators of Indoor Contamination and Moisture-Related Building Damage." *Environmental Science & Technology* 46 (11): 6088–95. https://doi.org/10.1021/es203782j.

Grafen, Markus, Konstantinos Nalpantidis, Frank Platte, Christian Monz, and Andreas Ostendorf. 2015. "Multivariate Characterization of a Continuous Soot Monitoring System Based on Raman Spectroscopy." *Aerosol Science and Technology* 49 (10): 997–1008. https://doi.org/10.1080/02786826.2015.1089352.

Grafen, Markus, Gustav Schweiger, Cemal Esen, and Andreas Ostendorf. 2018. "Time-Resolved Measurement of Elemental Carbon in Urban Environment: Comparison of Raman Backscattering and Aethalometer Results." *Journal of Aerosol Science* 117 (March): 34–43. https://doi.org/10.1016/j.jaerosci.2017.12.003.

Haagen-Smit, A. J. 1952. "Chemistry and Physiology of Los Angeles Smog." *Industrial & Engineering Chemistry* 44 (6): 1342–46. https://doi.org/10.1021/ie50510a045.

Haywood, J. M., and K. P. Shine. 1995. "The Effect of Anthropogenic Sulfate and Soot Aerosol on the Clear Sky Planetary Radiation Budget." *Geophysical Research Letters* 22 (5): 603–6. https://doi.org/10.1029/95GL00075.

Heinrich, Uwe, D L. Dungworth, F Pott, L Peters, C Dasenbrock, Karsten Levsen, Wolfgang Koch, O Creutzenberg, and Agnes Schulte. 1994. "The Carcinogenic Effects of Carbon Black Particles and Tar-Pitch Condensation Aerosol after Inhalation Exposure of Rats." *Annals of Occupational Hygiene* 38 (January): 351–56. https://doi.org/10.1093/annhyg/38.inhaled_particles_VII.351.

Hemby, James, Erika Sasser, Ken Adler, Susan Anenberg, Chad Bailey, Larry Brockman, Linda Chappell, et al. 2012. *Report to Congress on Black Carbon March 2012*.

Iida, Kenjiro, Mark R. Stolzenburg, and Peter H. McMurry. 2009. "Effect of Working Fluid on Sub-2 Nm Particle Detection with a Laminar Flow Ultrafine Condensation Particle Counter." *Aerosol Science and Technology* 43 (1): 81–96. https://doi.org/10.1080/02786820802488194.

"India: Air Quality Standards | Transport Policy." 2018. 2018. https://www.transportpolicy.net/standard/india-air-quality-standards/.

Jacobson, Mark Z. 2001. "Strong Radiative Heating Due to the Mixing State of Black Carbon in Atmospheric Aerosols." *Nature* 409 (6821): 695–97. https://doi.org/10.1038/35055518.

Jawhari, T., A. Roid, and J. Casado. 1995. “Raman Spectroscopic Characterization of Some Commercially Available Carbon Black Materials.” *Carbon* 33 (11): 1561–65. https://doi.org/10.1016/0008-6223(95)00117-V.

Jr, Wm E. Wilson, D. F. Miller, A. Levy, and R. K. Stone. 1973. “The Effect of Fuel Composition on Atmospheric Aerosol Due to Auto Exhaust.” *Journal of the Air Pollution Control Association* 23 (11): 949–56. https://doi.org/10.1080/00022470.1973.10469864.

Kangasluoma, Juha, Susanne Hering, David Picard, Gregory Lewis, Joonas Enroth, Frans Korhonen, Markku Kulmala, Karine Sellegri, Michel Attoui, and Tuukka Petäjä. 2017. “Characterization of Three New Condensation Particle Counters for Sub-3 Nm Particle Detection during the Helsinki CPC Workshop: The ADI Versatile Water CPC, TSI 3777 Nano Enhancer and Boosted TSI 3010.” *Atmospheric Measurement Techniques* 10 (6): 2271–81. https://doi.org/10.5194/amt-10-2271-2017.

Kim, Jung Hyeun, George W. Mulholland, Scott R. Kukuck, and David Y. H. Pui. 2005. “Slip Correction Measurements of Certified PSL Nanoparticles Using a Nanometer Differential Mobility Analyzer (Nano-DMA) for Knudsen Number From 0.5 to 83.” *Journal of Research of the National Institute of Standards and Technology* 110 (1): 31–54. https://doi.org/10.6028/jres.110.005.

Kulkarni, Pramod, Paul A. Baron, and Klaus Willeke. 2011. *Aerosol Measurement: Principles, Techniques, and Applications*. John Wiley & Sons.

Kulmala, Markku. 2003. “How Particles Nucleate and Grow.” *Science* 302 (5647): 1000–1001. https://doi.org/10.1126/science.1090848.

Lack, Daniel A., Hans Moosmüller, Gavin R. McMeeking, Rajan K. Chakrabarty, and Darrel Baumgardner. 2014. “Characterizing Elemental, Equivalent Black, and Refractory Black Carbon Aerosol Particles: A Review of Techniques, Their Limitations and Uncertainties.” *Analytical and Bioanalytical Chemistry* 406 (1): 99–122. https://doi.org/10.1007/s00216-013-7402-3.

Leamy, H. J. 1982. “Charge Collection Scanning Electron Microscopy.” *Journal of Applied Physics* 53 (6): R51–80. https://doi.org/10.1063/1.331667.

Legros, Gwenaelle, Ines Havet, Nigel Bruce, Sophie Bonjour, Kamal Rijal, and Minoru Takada. 2009. “The Energy Access Situation in Developing Countries: A Review Focusing on the Least Developed Countries and Sub-Saharan Africa.” *World Health Organization*.

Leibensperger, E. M., L. J. Mickley, D. J. Jacob, W.-T. Chen, J. H. Seinfeld, A. Nenes, P. J. Adams, D. G. Streets, N. Kumar, and D. Rind. 2011. “Climatic Effects of 1950–2050 Changes in US Anthropogenic Aerosols – Part 1: Aerosol Trends and Radiative Forcing.” *Atmospheric Chemistry and Physics Discussions* 11 (8): 24085–125. https://doi.org/10.5194/acpd-11-24085-2011.

Lohmann, U, and J Feichter. 2005. “Global Indirect Aerosol Effects: A Review.” *Atmos. Chem. Phys.*, 23. https://doi.org/10.5194/acpd-4-7561-2004.

Lohmann, Ulrike, Johann Feichter, Joyce Penner, and Richard Leaitch. 2000. "Indirect Effect of Sulfate and Carbonaceous Aerosols: A Mechanistic Treatment." *Journal of Geophysical Research: Atmospheres* 105 (D10): 12193–206. https://doi.org/10.1029/1999JD901199.

Madhavi Latha, K., and K. V. S. Badarinath. 2003. "Black Carbon Aerosols over Tropical Urban Environment—a Case Study." *Atmospheric Research* 69 (1): 125–33. https://doi.org/10.1016/j.atmosres.2003.09.001.

Maricq, M. Matti, Diane H. Podsiadlik, and Richard E. Chase. 2000. "Size Distributions of Motor Vehicle Exhaust PM: A Comparison Between ELPI and SMPS Measurements." *Aerosol Science and Technology* 33 (3): 239–60. https://doi.org/10.1080/027868200416231.

Moore, R. M., D. E. Oram, and S. A. Penkett. 1994. "Production of Isoprene by Marine Phytoplankton Cultures." *Geophysical Research Letters* 21 (23): 2507–10. https://doi.org/10.1029/94GL02363.

National Aerosol Association. 2014. "History of the Aerosol | National Aerosol Association (NAA)." 2014. http://www.nationalaerosol.com/history-of-the-aerosol/.

Novakov, T., and C. E. Corrigan. 1996. "Cloud Condensation Nucleus Activity of the Organic Component of Biomass Smoke Particles." *Geophysical Research Letters* 23 (16): 2141–44. https://doi.org/10.1029/96GL01971.

Patrick Arnott, W., Hans Moosmüller, C. Fred Rogers, Tianfeng Jin, and Reinhard Bruch. 1999. "Photoacoustic Spectrometer for Measuring Light Absorption by Aerosol: Instrument Description." *Atmospheric Environment* 33 (17): 2845–52. https://doi.org/10.1016/S1352-2310(98)00361-6.

Petzold, A., J. A. Ogren, M. Fiebig, P. Laj, S.-M. Li, U. Baltensperger, T. Holzer-Popp, et al. 2013. "Recommendations for Reporting "Black Carbon" Measurements." *Atmospheric Chemistry and Physics* 13 (16): 8365–79. https://doi.org/10.5194/acp-13-8365-2013.

Petzold, Andreas, and Markus Schönlinner. 2004. "Multi-Angle Absorption Photometry—a New Method for the Measurement of Aerosol Light Absorption and Atmospheric Black Carbon." *Journal of Aerosol Science* 35 (4): 421–41. https://doi.org/10.1016/j.jaerosci.2003.09.005.

Phairuang, Worradorn, Panwadee Suwattiga, Thaneeya Chetiyanukornkul, Surapa Hongtieab, Wongpun Limpaseni, Fumikazu Ikemori, Mitsuhiko Hata, and Masami Furuuchi. 2019. "The Influence of the Open Burning of Agricultural Biomass and Forest Fires in Thailand on the Carbonaceous Components in Size-Fractionated Particles." *Environmental Pollution* 247 (April): 238–47. https://doi.org/10.1016/j.envpol.2019.01.001.

Rosen, H., and T. Novakov. 1977. "Raman Scattering and the Characterisation of Atmospheric Aerosol Particles." *Nature* 266 (5604): 708. https://doi.org/10.1038/266708a0.

Sadezky, A, H Muckenhuber, Hinrich Grothe, Reinhard Niessner, and Ulrich Pöschl. 2005. "Raman Microspectroscopy of Soot and Related Carbonaceous Materials: Spectral

Analysis and Structural Information." *Carbon* 43 (July): 1731–42. https://doi.org/10.1016/j.carbon.2005.02.018.

Sandradewi, Jisca, Andre S. H. Prévôt, Sönke Szidat, Nolwenn Perron, M. Rami Alfarra, Valentin A. Lanz, Ernest Weingartner, and Urs Baltensperger. 2008. "Using Aerosol Light Absorption Measurements for the Quantitative Determination of Wood Burning and Traffic Emission Contributions to Particulate Matter." *Environmental Science & Technology* 42 (9): 3316–23. https://doi.org/10.1021/es702253m.

Seinfeld, John H., and Spyros N. Pandis. 2016. *Atmospheric Chemistry and Physics: From Air Pollution to Climate Change*. John Wiley & Sons.

Slowik, Jay G., Eben S. Cross, Jeong-Ho Han, Paul Davidovits, Timothy B. Onasch, John T. Jayne, Leah R. Williams, et al. 2007. "An Inter-Comparison of Instruments Measuring Black Carbon Content of Soot Particles." *Aerosol Science and Technology* 41 (3): 295–314. https://doi.org/10.1080/02786820701197078.

Sobanska, Sophie, HeeJin Hwang, Marie Choël, Hae-Jin Jung, Hyo-Jin Eom, HyeKyeong Kim, Jacques Barbillat, and Chul-Un Ro. 2012. "Investigation of the Chemical Mixing State of Individual Asian Dust Particles by the Combined Use of Electron Probe X-Ray Microanalysis and Raman Microspectrometry." *Analytical Chemistry* 84 (7): 3145–54. https://doi.org/10.1021/ac2029584.

"Standards - Air Quality - Environment - European Commission." 2018. 2018. http://ec.europa.eu/environment/air/quality/standards.htm.

Sze, S. -K., N. Siddique, J. J. Sloan, and R. Escribano. 2001. "Raman Spectroscopic Characterization of Carbonaceous Aerosols." *Atmospheric Environment* 35 (3): 561–68. https://doi.org/10.1016/S1352-2310(00)00325-3.

Takahama, Satoshi, Ann M. Dillner, Andrew T. Weakley, Matteo Reggente, Charlotte Bürki, Mária Lbadaoui-Darvas, Bruno Debus, Adele Kuzmiakova, and Anthony S. Wexler. 2019. "Atmospheric Particulate Matter Characterization by Fourier Transform Infrared Spectroscopy: A Review of Statistical Calibration Strategies for Carbonaceous Aerosol Quantification in US Measurement Networks." *Atmospheric Measurement Techniques* 12 (1): 525–67. https://doi.org/10.5194/amt-12-525-2019.

Tavakoli, Farzan, and Jason S. Olfert. 2014. "Determination of Particle Mass, Effective Density, Mass–Mobility Exponent, and Dynamic Shape Factor Using an Aerodynamic Aerosol Classifier and a Differential Mobility Analyzer in Tandem." *Journal of Aerosol Science* 75 (September): 35–42. https://doi.org/10.1016/j.jaerosci.2014.04.010.

Tegen, Ina, and Kerstin Schepanski. 2018. "Climate Feedback on Aerosol Emission and Atmospheric Concentrations." *Current Climate Change Reports* 4 (1): 1–10. https://doi.org/10.1007/s40641-018-0086-1.

Tittarelli, A., A. Borgini, M. Bertoldi, E. De Saeger, A. Ruprecht, R. Stefanoni, G. Tagliabue, P. Contiero, and P. Crosignani. 2008. "Estimation of Particle Mass Concentration in Ambient Air Using a Particle Counter." *Atmospheric Environment* 42 (36): 8543–48. https://doi.org/10.1016/j.atmosenv.2008.07.056.

TSI Incorporated. 2016. *Electrostatic Classifier Model 3082 Scanning Mobility Particle Aizer(SMPS) Spectrometer Model 3938 Operation and Service Manual*.

Tuch, Th., P. Brand, H. E. Wichmann, and J. Heyder. 1997. “Variation of Particle Number and Mass Concentration in Various Size Ranges of Ambient Aerosols in Eastern Germany.” *Atmospheric Environment* 31 (24): 4193–97. https://doi.org/10.1016/S1352-2310(97)00260-4.

US EPA, OAR. 2014. “NAAQS Table.” Policies and Guidance. US EPA. April 10, 2014. https://www.epa.gov/criteria-air-pollutants/naaqs-table.

Users, TTY, Lawrence J Hogan, Boyd K Rutherford, and Ben Grumbles. 2018. “MARYLAND DEPARTMENT OF THE ENVIRONMENT,” 112.

World Health Organization, ed. 2006. *Air Quality Guidelines: Global Update 2005: Particulate Matter, Ozone, Nitrogen Dioxide, and Sulfur Dioxide*. Copenhagen, Denmark: World Health Organization.

Yang, Wei, and Stanley T. Omaye. 2009. “Air Pollutants, Oxidative Stress and Human Health.” *Mutation Research/Genetic Toxicology and Environmental Mutagenesis*, Oxidative Stress and Mechanisms of Environmental Toxicity, 674 (1): 45–54. https://doi.org/10.1016/j.mrgentox.2008.10.005.

Presentations

Real-Time Aerosol Particle Measurement Methods: Air Quality Analysis (Presentation, 1st annual Louis Stokes Alliance for Minority Participation Undergraduate Research Symposium, College Park, MD, December 2nd, 2017)

Real-Time Aerosol Particle Measurement Methods: Air Quality Analysis (Presentation, University of Maryland Eastern Shore Regional Research Symposium, Princess Anne, MD, April 17th, 2018)

Real-Time Aerosol Particle Measurement Methods: Air Quality Analysis (Poster, Undergraduate Research Day, College Park, MD, April 25th, 2018)

Real-Time Aerosol Particle Measurement Methods: Air Quality Analysis (Presentation, Junior Technical Meeting/ Puerto Rico Interdisciplinary Meeting, Mayaguez, PR, April 28th, 2018)

Raman Characterization of Black Carbon Particle Size (Poster, Army Research Lab Summer Research Poster Session, Adelphi, MD, August 2018)

Raman Intensities of Mobility-Size Selected Sub-micron Black Carbon Particles (Poster, American Geophysical Union Fall Meeting, Washington, D.C., December 12th, 2018)